

THE CLOSE COMPANION MASS-RATIO DISTRIBUTION OF INTERMEDIATE-MASS STARS

KEVIN GULLIKSON ¹, ADAM KRAUS ¹, AND SARAH DODSON-ROBINSON ²
Draft version November 6, 2018

ABSTRACT

Binary stars and higher-order multiple systems are an ubiquitous outcome of star formation, especially as the system mass increases. The companion mass-ratio distribution is a unique probe into the conditions of the collapsing cloud core and circumstellar disk(s) of the binary fragments. Inside $a \sim 1000$ AU the disks from the two forming stars can interact, and additionally companions can form directly through disk fragmentation. We should therefore expect the mass-ratio distribution of close companions ($a \lesssim 100$ AU) to differ from that of wide companions. This prediction is difficult to test using traditional methods, especially with intermediate-mass primary stars, for a variety of observational reasons. We present the results of a survey searching for companions to A- and B-type stars using the direct spectral detection method, which is sensitive to late-type companions within $\sim 1''$ of the primary and which has no inner working angle. We estimate the temperatures and surface gravity of most of the 341 sample stars, and derive their masses and ages. We additionally estimate the temperatures and masses of the 64 companions we find, 23 of which are new detections. We find that the mass-ratio distribution for our sample has a maximum near $q \sim 0.3$. Our mass-ratio distribution has a very different form than in previous work, where it is usually well-described by a power law, and indicates that close companions to intermediate-mass stars experience significantly different accretion histories or formation mechanisms than wide companions.

Subject headings: binaries: spectroscopic, stars:early-type, stars:formation, stars:statistics

1. INTRODUCTION

Stellar multiplicity is an inevitable and common outcome of star formation, with roughly half of all solar-type field stars in binary or multiple systems (Raghavan et al. 2010) and an even higher fraction as the stellar mass increases (Zinnecker & Yorke 2007). Young stellar associations and clusters tend to have even higher multiplicity (Duchêne & Kraus 2013), indicating that stars often form in multiple systems that are subsequently destroyed by dynamical interactions as the cluster dissociates.

The overall multiplicity rate and the distributions of mass ratio, period, and eccentricity of a binary star population place important constraints on the mode of binary star formation. While the period and eccentricity are altered by dynamical processing in the birth cluster, the present-day mass ratio of a binary system is a direct result of its formation (Parker & Reggiani 2013). Most binary stars are thought to form via core fragmentation (Boss & Bodenheimer 1979; Boss 1986; Bate et al. 1995), in which a collapsing core fragments into two or more individual protostars. The number and initial masses of the fragments are set by the total core mass, as well as its rotation, turbulence, and its temperature and density structure. If the fragments are well separated ($a \gtrsim 1000$ AU), they will evolve independently of each other, accreting mass from the core material onto their own protostellar disks and then onto the protostars themselves. However close fragments ($a \sim 100$ AU) will interact with each other; the protostellar disk may be truncated, destabilized, or form into a circumbinary disk if the separation is small enough (Bate & Bonnell 1997). In addition, an

unstable disk can fragment to form low-mass companions (Kratter & Matzner 2006; Stamatellos & Whitworth 2011). The mass ratios of close companions formed via either mechanism should be affected by preferential accretion. Most work has suggested that the disk material will preferentially accrete onto the lower mass companion (Bate & Bonnell 1997; Bate et al. 2002); however, recent work has indicated that magnetic disk braking may result in preferential accretion onto the more massive component (Zhao & Li 2013) instead. In either case, we would expect to find a mass-ratio distribution for companions inside a few 100 AU that differs from that of companions on wider orbits where preferential accretion does not occur.

The mass ratio, period, and eccentricity distributions are well-known for solar type stars (Duquennoy & Mayor 1991; Raghavan et al. 2010) and cooler stars (Fischer & Marcy 1992; Delfosse et al. 2004). Interestingly, Reggiani & Meyer (2011), and later Reggiani & Meyer (2013), found that the mass-ratio distribution of field solar-type and M-dwarf stars is invariant to separation. The field M-dwarf semimajor axis distribution peaks near ~ 5 AU (Duchêne & Kraus 2013), with very few companions at separation $\gtrsim 100$ AU; the 27 stars used in the analysis by Reggiani & Meyer (2011) is unsufficient to compare the mass-ratio distribution inside ~ 100 AU with that outside it. However, the solar-type period distribution peaks near 45 AU (Raghavan et al. 2010), with roughly 40% of binary systems on orbits wider than 100 AU. The nondetection of a difference in mass-ratio distribution is significant, although with only 30 stars in the field sample it is difficult to completely rule out that such a difference exists.

All of the orbital distributions are much less certain for more massive stars. The reason for this is two-fold: first,

¹ University of Texas, Astronomy Department. 2515 Speedway, Stop C1400. Austin, TX 78712

² University of Delaware, Department of Physics and Astronomy, 217 Sharp Lab, Newark, DE 19716

more massive stars tend to be more distant than sun-like or low-mass stars, meaning many of the companions are angularly close to the primaries and difficult to detect with imaging techniques. Second, the primary stars tend to be rapid rotators, which limits radial velocity precision to $\sim 1 \text{ km s}^{-1}$ and causes the spectral lines of double-lined systems to blend. Radial velocity monitoring can only measure a mass ratio if spectral lines from both components are visible and separable; this typically suffers from the same flux ratio difficulty as imaging techniques.

Nonetheless, De Rosa et al. (2014) performed an adaptive optics imaging survey of nearby A-type stars, and found that the mass-ratio distribution is well-described by a power law with large slope, indicating a very strong preference for low-mass companions. They also found initial evidence that the mass-ratio distribution for companions inside 125 AU has a much shallower power law slope than that of wide companions, and is consistent with flat. Their close companion subsample contained only 18 binary systems, and the result is complicated by the inherent difficulty of detecting close companions with low mass ratios in an imaging survey.

Radial velocity monitoring surveys can detect much closer companions than imaging surveys, but are typically only complete to low-mass companions if the primary is a slow rotator. Chemically peculiar Am stars are typically associated with binary companions, and are slow rotators due to tidal braking; they thus form a highly biased sample of intermediate-mass stars. Nonetheless, it is interesting to note that they have a mass-ratio distribution which peaks near $q \sim 0.5$ (Vuissoz & Debernardi 2004), an entirely different form than the distribution found around chemically normal stars at wide separations.

In this paper, we describe a spectroscopic survey of nearby chemically normal, main sequence intermediate-mass stars ($M \approx 1.5 - 15 M_{\odot}$). We search for companions using the direct spectral detection technique (Gullikson et al. 2016), which has a separation-invariant detection rate for all separations inside $\sim 1''$. We describe the stellar sample and data used for the survey in Section 2, as well as the data reduction steps in the same section. Next, we describe the direct spectral detection method and tabulate the companion detections in Section 3. We estimate the mass and age of the sample stars in Section 4, and discuss the survey completeness in Section 5. Finally, we end with a derivation of the mass-ratio distribution from our sample in Section 6 and discuss its implications for binary formation in Section 7.

2. OBSERVATIONS AND DATA REDUCTION

The stellar sample for this survey is defined by the following criteria:

- $V < 6$ mag
- $v \sin i > 80 \text{ km s}^{-1}$
- Spectral Type A or B with the following additional constraints
 - Main Sequence
 - No spectral peculiarities except for ‘n’, which denotes broad lines.

The magnitude limit ensures that a sufficiently high signal-to-noise ratio can be achieved in a short period of time. It does introduce a Malmquist bias in the derived mass ratio, which we discuss and correct for in Section 6. Likewise, the $v \sin i$ limit makes accounting for the primary star spectrum in the companion search trivial; since most A- or B-type stars are rapid rotators, the cutoff removes less than half of the stars from the potential sample. We exclude pre-main sequence stars because both the primary and the companion mass would depend very strongly on young and uncertain ($\lesssim 1$ Myr) evolutionary models. Finally, we exclude post-main sequence stars from our sample because the binary flux ratio would be even less favorable to companion detection in an evolved star. Most of the spectral peculiarities denote narrow lines, which are already removed from the sample by the $v \sin i$ cut. The sample is given in Table 1. The spectral type, coordinates, V magnitude, and parallax are all adopted from the Simbad Database (Wenger et al. 2000), while the stellar effective temperature, surface gravity, masses, and ages are discussed in Section 4.

The sample, being comprised of early-type stars, is heavily biased towards young stars. The estimated ages range from about 10 Myr to 1 Gyr, with most falling in the range of a few tens or hundreds of Myrs. The sample also mostly contains nearby stars, although the magnitude limit provides a greater extent than a volume-limited survey would. The parallactic distances in our sample range from $\sim 15 - 2000$ pc. The maximum detectable separation, which we define as the point at which the companion is no longer guaranteed to fall on the spectrograph slit (see Section 2.1 for a description of the spectrographs we use), is $\sim 20 - 4000$ AU. The median parallactic distance in our sample is 95 pc, corresponding to a projected separation of ~ 200 AU. Most of the companions we are able to detect are close enough to have been impacted by the circumprimary disk, with 85% of the sample sensitive to companions inside 100 AU.

2.1. Spectroscopic Data

We use several high spectral resolution, cross-dispersed échelle spectrographs for this survey. We use the CHIRON spectrograph (Tokovinin et al. 2013) on the 1.5m telescope at Cerro Tololo Inter-American Observatory for most southern targets. This spectrograph is an $R \equiv \lambda/\Delta\lambda = 80000$ spectrograph with wavelength coverage from 450 - 850 nm, and is fed by a 2.7'' optical fiber. The data are automatically reduced with a standard CHIRON data reduction pipeline, but the pipeline leaves residuals of strong lines in adjacent orders. We therefore bias-correct, flat-field and extract the spectra with the optimum extraction technique (Horne 1986) using standard IRAF³ tasks, and use the wavelength calibration from the pipeline reduced spectra.

For the northern targets, we use a combination of the High Resolution Spectrograph (HRS, Tull 1998) on the Hobby Eberly Telescope, and the Tull coude (TS23, Tull et al. 1995) and IGRINS (Park et al. 2014) spectrographs, both on the 2.7m Harlan J. Smith Telescope. All three

³ IRAF is distributed by the National Optical Astronomy Observatories, which are operated by the Association of Universities for Research in Astronomy, Inc., under cooperative agreement with the National Science Foundation.

northern instruments are at McDonald Observatory. For the HRS, we use the $R = 60000$ setting with a $2''$ fiber, and with wavelength coverage from 410–780 nm. We bias-correct, flat-field, and extract the spectra using an IRAF pipeline very similar to the one we use for the CHIRON data. The HRS spectra are wavelength-calibrated using a Th-Ar lamp observed immediately before or after the science observations.

For the TS23 spectrograph, we use a $1.2''$ slit in combination with the E2 échelle grating (53 grooves/mm, blaze angle 65°), yielding a resolving power of $R = 60000$ and a wavelength coverage from 375–1020 nm. We reduce the data using an IRAF pipeline very similar to the ones we use for CHIRON and HRS, and wavelength calibrate using a Th-Ar lamp observed immediately before the science observations.

IGRINS has a single setting with $R = 40000$. It has complete wavelength coverage from 1475–2480 nm, except in the telluric water band from 1810–1930 nm. Each star is observed in an ABBA nodding mode, and reduced using the standard IGRINS pipeline (Lee 2015). The standard pipeline uses atmospheric OH emission lines as well as a Th-Ar calibration frame to calibrate the wavelengths; we further refine the wavelength solution using telluric absorption lines in the science spectrum.

After reducing the data, we fit and remove the telluric spectrum using the TelFit code (Gullikson et al. 2014). We fit each échelle order affected by telluric absorption independently from each other to get the best removal. The telluric correction is critical for IGRINS spectra, where every order is dominated by telluric absorption lines. For the optical spectra, it is less critical but allows us to use some of the redder orders than we otherwise would be able to. For unsaturated lines, the best-fit telluric model reproduces the data to within $\sim 1 - 5\%$ of the continuum level.

We give the spectroscopic observation log in Table 2. We calculate the signal-to-noise ratio (the “snr” column) for the optical instruments (CHIRON, TS23, and HRS) as the median of the extracted flux divided by its uncertainty for each pixel from the échelle order nearest 675 nm. For the IGRINS instrument, we calculate the signal-to-noise ratio from the order nearest 2200 nm.

2.2. Imaging Data

As part of the follow-up effort, we used the NIRI instrument behind the Altair adaptive optics system on the Gemini North Telescope. For each star listed in Table 3, we obtained 25 images in 5 dithering positions. We used the K-continuum band centered on $2.2718 \mu\text{m}$ and a variety of exposure times and dates (listed in Table 3). Because the targets are all extremely bright, we used the high read noise and high flux detector settings to allow for very short co-add exposure times and to prevent saturation. We reduced the data using the Gemini set of IRAF tasks, which include steps for nonlinearity correction, flat-fielding, sky subtraction, and co-addition of the dither frames.

We measure the flux and position of both stars by fitting a 2D Moffat function (Moffat 1969) to both stars simultaneously, constraining the shape parameters for both functions to be the same. The ratio of the amplitudes gives the magnitude difference, and the pixel locations along with the detector pixel scale gives the separation and position angle between the stars. We note that the goal of these images was confirmation and we did not observe any reference targets to make a distortion map and correct the image rotation. The uncertainty in position angle and to a lesser degree separation quoted in Table 3 is likely underestimated.

3. COMPANION SEARCH

We search for stellar companions to our sample stars using the direct spectral detection technique, described in detail in Gullikson et al. (2016). In short, we unsharp-mask each spectrum using a gaussian filter with width proportional to the primary star $v \sin i$ to remove the broad lines from the primary star. We then cross-correlate each échelle order of each filtered spectrum against a large grid of Phoenix model spectra (Husser et al. 2013) with the following parameters:

- $T_{\text{eff}} = 3000 - 12000 \text{ K}$, in steps of 100 K
- $[\text{Fe}/\text{H}] = -0.5, 0.0, +0.5$
- $v \sin i = 1, 5, 10, 20, 30 \text{ km s}^{-1}$

In order to be sensitive to hot companions, we additionally cross-correlate the spectra against a second grid of Kurucz model spectra (Castelli & Kurucz 2003). The change in model is necessary because the Phoenix model library does not extend beyond 12000 K. The Kurucz grid is defined as follows:

- $T_{\text{eff}} = 9000 - 30000 \text{ K}$, in steps of 1000 K
- $[\text{Fe}/\text{H}] = -0.5, 0.0, +0.5$
- $v \sin i = 1, 5, 10, 20, 30, 40, 50 \text{ km s}^{-1}$

We combine the cross-correlation functions for all orders using both a simple average and the maximum-likelihood weighting scheme (Zucker 2003). A companion detection is denoted by a strong peak in the combined cross-correlation function (CCF). While the maximum-likelihood scheme produces detections with much higher significance, it also magnifies spurious peaks and so has a larger false-positive rate. For this reason, we use the simple average CCFs in all further analysis.

The peak height in the CCF as a function of the stellar model acts in a similar way to the more typical χ^2 map of parameter space. More concretely, as the stellar model template gets closer to the true companion spectrum, the CCF peak gets higher. We can therefore measure the companion temperature and, to a lesser degree its metallicity and $v \sin i$, in a single spectrum. We calculate the measured temperature (T_m) and variance (σ_T^2) as a weighted sum near the grid point with the highest CCF peak value, weighting by the peak CCF height at each temperature (C_i):

$$T_m = \sum_i C_i T_i / \sum_i C_i \quad (1)$$

$$\sigma_T^2 = \frac{\sum_i C_i (T_i - T_m)^2}{\sum_i C_i - \sum_i C_i^2 / \sum_i C_i} \quad (2)$$

Typical uncertainties are on the order of 200 K. In the case of multiple observations for the same star, we use

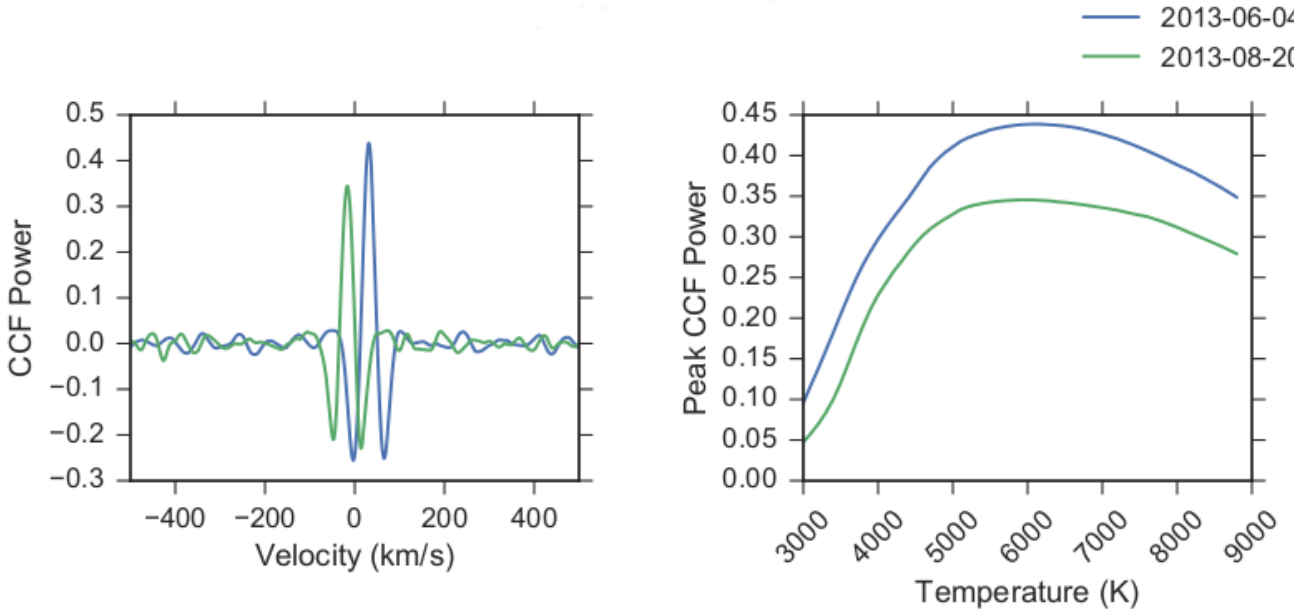


FIG. 1.— *Left:* Cross-correlation function between the observed spectra of HIP 109139 and a 5700 K Phoenix model spectra. The detection at two dates shows significant velocity variation, indicating orbital motion with a short period. *Right:* Peak CCF height as a function of Phoenix model spectra template temperature. The maxima of the curves indicate the temperature of the companion.

the variance-weighted mean of the individually measured temperatures.

Imperfect stellar models cause a bias between the true companion temperature and the measured temperature (T_m). This bias is most pronounced at low temperatures, where the difficult-to-model molecular absorption becomes important. We correct for the bias by applying the linear calibrations developed in Gullikson et al. (2016). These calibrations are only valid for companions with $3000 < T_{\text{eff}} < 7000 K$; for detections at hotter temperatures we assume that the temperature which produces the maximum CCF peak is an *unbiased* estimator of the true companion temperature.

We list the companion detections in Table 4, and report the estimate of the companion temperature, $v \sin i$, and metallicity derived from the model parameters which produce the largest CCF peak. The $v \sin i$ and metallicity values do not have uncertainties and should only be taken as a rough estimate of the true value. The mean and standard deviation of the companion metallicities is -0.29 ± 0.30 ; the marginal bias towards low metallicities is most likely a measurement bias and does not reflect the true companion population (Gullikson et al. 2016). We show the detection CCFs and a plot of peak CCF height as a function of model temperature for HIP 109139 in Figure 1. Similar figures for all companions are available in the supplementary files.

We have follow-up spectroscopy for 15/23 of the new companions to confirm their existence. In most cases, there is a clear shift in the radial velocity of the companion, indicating that it is orbiting the target star and is not a foreground or background contaminant (See Figure 1). Two of the new detections (companions to HIPs 38593 and 79404) were detected twice but not in a third attempt, most likely because the third spectrum had low signal-to-noise. The companion to HIP 93805, at $\sim 4000 K$, was detected twice with near-infrared IGRINS but

not the optical CHIRON instrument that is less sensitive to cool companions than IGRINS. Two of the companions with only one detection were observed at least twice (HIPs 19949 and HIP 23362); both of the non-detections are from the IGRINS instrument, which is less sensitive to hot companions with rapid rotation speeds because there are far fewer spectral lines of the companion in the near-infrared than there are in the optical.

In addition to the spectroscopic follow-up, we obtained Gemini/NIRI adaptive optics imaging data for 18 of the northern companions, and were able to resolve 7 of them. We show the separation, position angle, and magnitude difference measurements in Table 3, and display the images in Figure 2. We also derive the projected separation in AU and the companion mass from the images. We calculate the separation from the measured angular separation and the Hipparchos parallax (van Leeuwen 2007). We calculate the companion mass and uncertainties from 1000 samples of the magnitude difference measurement and the primary star mass, temperature, age, and radius (see Section 4). For each sample, we use a grid of Kurucz stellar model spectra (Castelli & Kurucz 2003) and the pysynphot code⁴ to determine the companion temperature needed to replicate the observed magnitude difference. We estimate the companion radius by interpolating solar metallicity Dartmouth isochrones (Dotter et al. 2008) from the companion temperature and system age sample. We convert the best temperature to a companion mass using the same isochrone grid. The masses derived from the imaging data have very large uncertainties because the primary star property estimates that they depend on are very uncertain. The imaging masses agree with the spectroscopically-derived masses

⁴ pysynphot is a python package to perform synthetic photometry, and is available at this url: <https://pypi.python.org/pypi/pysynphot>

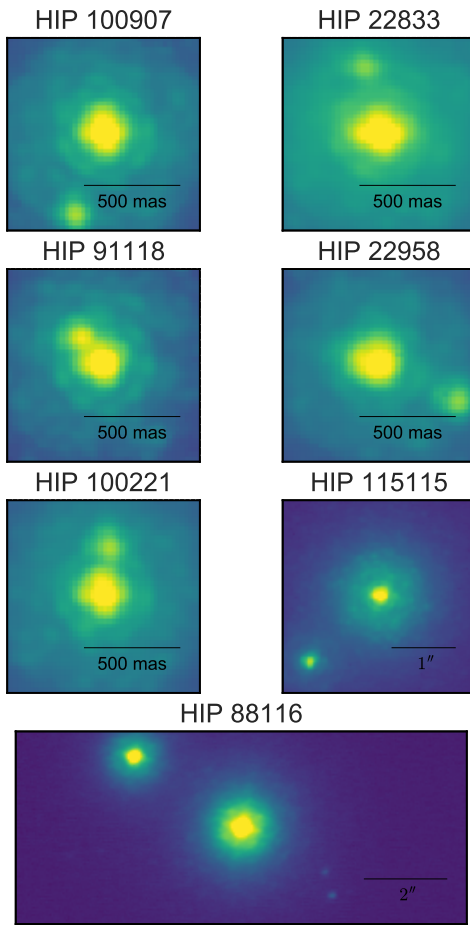


FIG. 2.— Detection images for all stars in which we detect a companion in the follow-up NIRI data. There are several nearby sources for HIP 88116, none of which are the source we detect in the spectroscopic data (see Section 3).

in Table 4, with the exception of HIP 115115 which has a much higher mass from the imaging data than the spectroscopic data. The spectroscopic masses for all stars are more reliable, since they are less model-dependent.

One star in the imaging sample, HIP 88116, has several nearby sources in the image. We quote the magnitude difference and separation of the brightest source in Table 3, but stress that *none* of the visible sources is likely to be the companion we see in the spectroscopic data. The two epochs of spectroscopic data show a radial velocity shift of $\Delta v = 30.7 \text{ km s}^{-1}$ over the course of roughly one year; this orbital motion is much too large to be consistent with any of the companions visible in the image (all with separations $> 1''$ and projected separations $> 300 \text{ AU}$).

4. SAMPLE STAR PARAMETERS

In order to convert from companion temperature to mass ratio, we first need an estimate of the primary mass. In addition, since the primary stars in our survey have short main-sequence lifetimes, some companions may still be contracting onto the main sequence and so an age estimate for the system is necessary to convert from companion temperature to mass.

About half of our sample stars have robust mass and age estimates from Strömgren uvby β photometry (David & Hillenbrand 2015). For those that do not, we estimate the mass and age of the system from our spectra. We first cross-correlate the data against a grid of solar metallicity Kurucz model spectra (Castelli & Kurucz 2003) spanning

- $7000 \text{ K} < T_{\text{eff}} < 30000 \text{ K}$ in steps of 500 K for $T < 10000 \text{ K}$, and in steps of 1000 K for hotter templates.
- $3.0 < \log g < 4.5$ in steps of 0.5 dex
- $75 < v \sin i < 300 \text{ km s}^{-1}$ in steps of 25 km s^{-1}

For the optical data, we use the blue échelle orders ($\lambda < 5550 \text{\AA}$). We ignore the strong hydrogen Balmer lines in the spectrum because they span several échelle orders and make continuum normalization very difficult, potentially biasing the result. There are sufficient metal lines in the optical spectra that the resulting CCF always has a very strong peak at the radial velocity of the primary star. The near-infrared IGRINS spectra have very few strong metal lines; we use the subset from $1.51 - 1.73 \mu\text{m}$ that is dominated by hydrogen Brackett lines for these spectra. Similar to the companion search, we estimate the temperature and surface gravity of the stars from the CCF with the largest peak. We adopt the following errors on the temperature and surface gravity, which are based on the grid step size and are somewhat more pessimistic than typical uncertainties seen in the literature for A- and B-type stars (e.g. Aydi et al. 2014; David & Hillenbrand 2015):

$$\sigma_T = \begin{cases} 500 \text{ K} & T < 10000 \text{ K} \\ 1000 \text{ K} & T \geq 10000 \text{ K} \end{cases} \quad (3)$$

$$\sigma_{\log g} = 0.25 \quad (4)$$

The IGRINS parameters are less reliable because they rely almost solely on the hydrogen Brackett lines that span an entire échelle order, so we double the uncertainty on the IGRINS-derived temperature and surface gravity. Additionally, we throw out the IGRINS parameters if the star was also observed by one of the optical instruments in our survey. For stars observed multiple times, we use the average parameters and reduce the uncertainties accordingly.

Next, we use Padova stellar evolutionary tracks (Bressan et al. 2012) and the isochrones code (Morton 2015) to estimate the mass and age of the system from the measured temperature and surface gravity. As a consistency check, we also interpolate from a table of stellar properties as a function of spectral type (Pecaut & Mamajek 2013) to estimate the primary mass from the published spectral types. We show the comparison in Figure 3. We estimate uncertainties in the spectral type mass by assuming a spectral type uncertainty of ± 0.5 spectral types and propagating to mass. There is excellent agreement between the masses we measure and the spectral type masses.

We show the temperature, surface gravity, mass, and age estimates for most of our sample stars in Table 1. We do not give parameters for the few stars that show strong discrepancies with the spectral-type estimate, most of

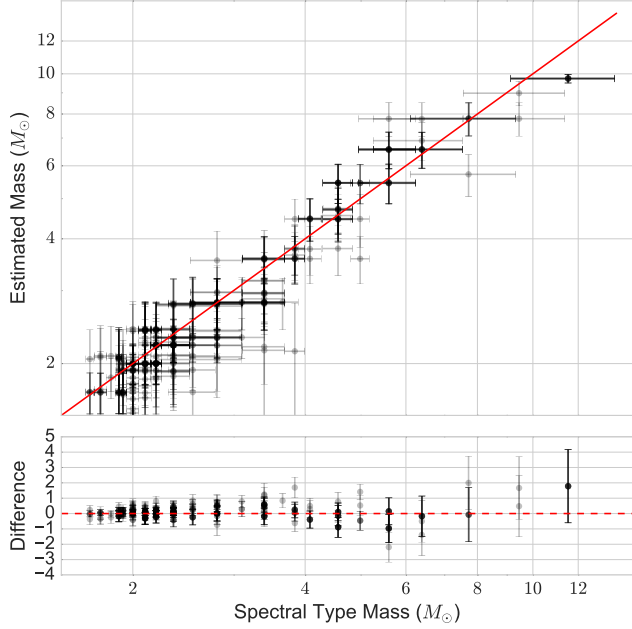


FIG. 3.— Comparison of primary star masses derived from our cross-correlation analysis and Padova isochrones (Bressan et al. 2012) with those expected from the published spectral type. There is excellent agreement between the two measures across the entire range of masses.

which are early B-stars that have temperatures higher than the maximum grid temperature of 30000 K.

5. SURVEY COMPLETENESS

The detectability of a companion mostly depends on its temperature: cooler companions emit much less light and so are increasingly lost in the Poisson noise from the primary star spectrum. A companion with a high rotation rate is also more difficult to detect because the cross-correlation function gets most of its power from narrow spectral lines.

5.1. Injection and Recovery Tests

To quantify the detection rate as a function of companion temperature and $v \sin i$, we performed a series of injection and recovery experiments. We started by creating synthetic binary star observations from each of our observed spectra. We made two distinct grids of companion stars: a low temperature grid spanning

- $3000 \text{ K} < T_{\text{eff}} < 6500 \text{ K}$ in steps of 100 K
- $0 \text{ km s}^{-1} < v \sin i < 50 \text{ km s}^{-1}$ in steps of 10 km s^{-1}

and a high temperature grid spanning

- $7000 \text{ K} < T_{\text{eff}} < 12000 \text{ K}$ in steps of 1000 K
- $100 \text{ km s}^{-1} < v \sin i < 250 \text{ km s}^{-1}$ in steps of 50 km s^{-1}

For each grid point, we added a solar metallicity Phoenix model spectrum to the observed data after scaling to replicate the expected flux between a main sequence companion of the model temperature and the known target

star spectral type. If the target star had known companions within 3'', we included the expected flux from the companion when computing the flux ratio. We repeated each grid point at different radial velocities spanning $-400 \text{ km s}^{-1} < v < 400 \text{ km s}^{-1}$ in 50 km s^{-1} steps to sample the noise properties of the spectra and estimate a probability of detection at each point.

Next, we cross correlated all of the synthetic observations against the Phoenix model template that was used to construct them. We counted the companion as detected if the highest point in the resulting CCF was found at the correct radial velocity, and if the peak had a significance of $> 5\sigma$, where σ is the standard deviation of the CCF for points more than 100 km s^{-1} away from the peak. We combined all of the radial velocity trials for each grid point to estimate a probability of detection at that grid point:

$$P(\text{detection}) = \frac{N_{\text{detected}}}{N_{\text{rv}}} \quad (5)$$

where $N_{\text{rv}} = 17$ is the number of radial velocity trial points.

Finally, we interpolated between the grid points using a linear radial basis function interpolator (Figure 4). In order to extrapolate from our grids to estimate the detection rate at high temperature and low $v \sin i$ and at low temperature and high $v \sin i$, we made the following assumptions about the shape of the two-dimensional detection rate surface: First, we assume that if no companions are detected at temperature T and rotation speed $v \sin i = 50 \text{ km s}^{-1}$, then no companions will be detected at the same temperature and faster rotation speeds (upper left points in Figure 4). Likewise, we assumed that if all companions are detected at temperature $T = 6500 \text{ K}$ and rotation speed $v \sin i$, then all companions with the same $v \sin i$ and larger temperature will also be detected (lower right points in Figure 4). The detection rate of hot companions is affected by two factors: the increased flux from the companion makes detection easier, while the decreasing number of spectral lines in the companion spectrum makes detection more difficult. If the latter factor is more important, then the assumption we made about the shape of the detection surface is incorrect. We therefore tested the assumption with a small subset of injection and recovery tests, and found that the second assumption we make is valid.

Figure 4 shows a clear diagonal dividing line between hot, slow rotators that are always detected and cool, fast rotators that never are. Additionally the figure shows that very fast rotators are never detected, regardless of their temperature, because the signal is completely removed when we unsharp-mask the data (see Section 3).

5.2. Marginalization

By sampling a suitable distribution of $v \sin i$ values for a star of each temperature, we marginalize over the rotation speed:

$$Q(T) = \sum_k Q(T, v_k) v_k \quad (6)$$

where $Q(T, v)$ is the surface plotted in Figure 4 and v_k are the samples from the distribution of $v \sin i$. For $T < 6000$

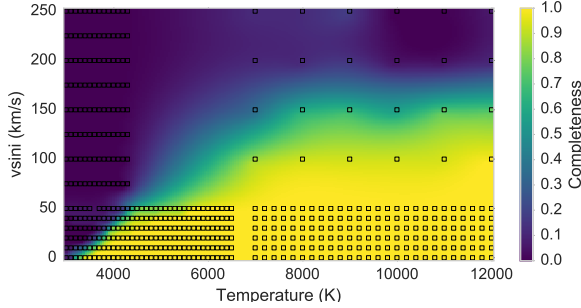


FIG. 4.— Detection rate as a function of companion temperature and $v \sin i$ for HIP 24244. All companions that are shaded yellow are detectable, while companions in the purple region are never detectable. The grids of squares in the lower left and upper right show the low temperature and high temperature grid points we used in the sensitivity analysis. The remaining squares come from assumptions about the shape of the detection rate surface and allow us to fully interpolate (see text for details).

K, we sample $v \sin i$ using the gyrochronology relation given in Barnes (2010):

$$\frac{k_C t}{\tau} = \ln\left(\frac{P}{P_0}\right) \frac{k_I k_C}{2\tau^2} (P^2 - P_0^2) \quad (7)$$

In Equation 7, k_C and k_I are constants fit to data with known ages and rotation periods, P and P_0 are respectively the current and zero-age main sequence (ZAMS) rotation periods, τ is the convective turnover time scale and t is the current age of the star. We use the same values that Barnes (2010) use for the constants:

- $k_C = 0.646$ day/Myr
- $k_I = 452$ Myr/day

We estimate the convective timescale (τ) by interpolating Table 1 of Barnes & Kim (2010). We then randomly draw a system age t from its probability distribution function (see Section 4 and Table 1). Young stars have rotation periods in the range of 0.2 to 10 days (Bouvier et al. 2014), so we randomly choose an initial rotation period P_0 from a log-uniform distribution in this range for each age sample. Equation 7 then gives a current rotation period for each sample, which we convert to an equatorial velocity with the stellar radius R . We estimate R by interpolating Dartmouth pre main sequence isochrones (Dotter et al. 2008) using the companion temperature and system age. We finally convert to projected velocity $v \sin i$ by randomly sampling a uniform distribution for the inclination $\sin i$.

The gyrochronology relations are invalid for stars with $T \gtrsim 6250$ K, the canonical limit at which the convective zone is too small to efficiently remove angular momentum to the stellar wind and spin down the star (Pinsonneault et al. 2001). Zorec & Royer (2012) fit Maxwellian distributions to the equatorial velocity of A- and B-type stars in several mass bins. For $T > 7000$ K, we linearly interpolate the fit parameters as a function of mass and sample the resulting Maxwellian probability density function.

Typical velocities from the gyrochronology relationships are $10 - 20$ km s $^{-1}$, while the Maxwellian velocity distributions have typical velocities ~ 100 km s $^{-1}$. We transition between the two regimes for temperatures in

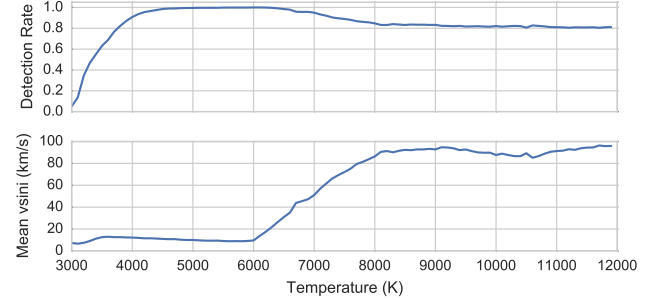


FIG. 5.— Marginalized detection rate for the same star as shown in Figure 4. The fall in detection rate towards hotter stars is caused by the increase in typical rotational speeds.

the range 6000 K $<$ T $<$ 7000 K by first estimating the equatorial velocities from the gyrochronology relationship (Equation 7) at $T = 6000$ K. We then fit the velocities to a Maxwellian distribution, and add the result to the tabulated parameters from (Zorec & Royer 2012). With the extended table, we treat stars in the transition range the same way we treat hot stars.

We show the marginalized detection rate and mean value of $v \sin i$ as a function of temperature in Figure 5. Both the detection rate and the average $v \sin i$ are smoothly varying, and show the expected behaviour with temperature. The detection rate falls with hotter temperatures because the companions are expected to be fast rotators, which are more difficult to detect.

5.3. Conversion to Mass Ratio

The result of the previous analysis is a series of estimates for the detection rate as a function of companion temperature for each observation of each star. We convert companion temperature to mass by interpolating Table 5 of Pecaut & Mamajek (2013). Next, we estimate the primary mass for each star as the median of the mass samples developed in Section 4. We then convert each detection rate curve to be a function of mass ratio ($Q_j(q)$, where j denotes the j th star in the sample), and linearly interpolate onto a grid in mass ratio from $0 < q_i < 1$. Finally, we combine the detection rate curves for each star *with no companion detection in our data* into an estimate of the survey-wide completeness by taking the average of the detection rate for all stars:

$$Q(q_i) = \frac{1}{N_i} \sum_j Q_j(q_i) \quad (8)$$

In the equation above, N_i is the number of sample stars that contain an estimate for $Q(q_i)$ without extrapolating. For $q_i \sim 0.2$, N_i is near the total sample size. However, N_i falls for both low and high q , since a 3000 K/12000 K companion has a mass ratio $q = 0.08/2.0$ for an A9V primary, but $q = 0.007/0.19$ for a B0V primary. Our sensitivity analysis therefore does not sample large mass ratios around the very early-type primary stars in the sample, and does not sample very low mass ratios around late-type primary stars.

Gullikson et al. (2016) used a very similar method to search for known companions to A- and B-type stars, and found that the detection rate is high for G- and K-dwarf companions but very low for hot companions. The search grid used in this work includes much hotter tempera-

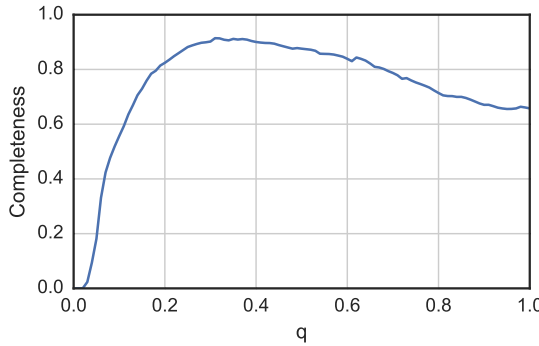


FIG. 6.— Survey completeness as a function of mass ratio (q).

tures, and we have several detections of hot companions (see Table 4). We test to determine if the completeness is reasonable at large mass ratios by comparing to known binary systems. We detect 15 of the 25 stars in our sample with a hot ($T > 7000$ K) companion in either the Washington Double Star Catalog (Mason et al. 2014) or the Ninth Catalog of Spectroscopic Binary Orbits (Pourbaix et al. 2009). The completeness function for hot, roughly equal-mass companions suggests the probability of detection is $\sim 80\%$, which is still incompatible with our low detection rate. The discrepancy may be due to an underestimate of the typical rotation rates for hot stars, which we use when marginalizing out the dependence on $v \sin i$. Additionally, rapidly rotating companions, especially when they have a similar temperature to the primary, are more difficult to detect if they have a small radial velocity offset from the primary star. While the injection and recovery experiments do sample velocity space to account for this, they may be over-sampling companions with very large velocity offsets and producing anomalously high detection rates. We account for the discrepancy by introducing a scaling factor: we multiply the estimated detection rate for all companions with $T > 7000$ K by $f = 0.8$.

We show the resulting total survey completeness in Figure 6. The completeness falls very rapidly towards low mass ratios, although we are still $\sim 60\%$ complete at $q = 0.1$. The slow fall-off towards large mass ratios is caused by a combination of the scale factor described above and the inherent difficulty of detecting rapidly rotating companions (see Figure 5). The detection rate at large mass ratios is now $\sim 0.6 - 0.7$, which is consistent with our 15/25 empirical detection rate.

6. MASS-RATIO DISTRIBUTION

We are now finally in a position to estimate the mass-ratio distribution for our sample. We estimate the mass for each detected companion star by sampling the temperatures given in Table 4 as a gaussian, and converting each temperature sample into a mass sample. We do the conversion to mass both by interpolating Table 5 from Pecaut & Mamajek (2013), and by interpolating from temperature and system age (see Section 4) to mass with Dartmouth isochrones (Dotter et al. 2008). Both methods give similar results in most cases. Since the isochrone masses are more accurate at young ages, we use them throughout the analysis that follows. We sample the mass ratio of the system by dividing the companion

mass samples by samples of the primary mass (Section 4). We denote the n th mass ratio sample for the k th star as $q_k^{(n)}$, and denote the number of these samples as N_k .

We do not use systems with more than one companion, unless the wider companion is separated by $> 10''$ from the primary star. We mark the 50 companions we use in the mass ratio analysis with the fourth column of Table 4. Many of the companions we use in the analysis only have one detection in our data; 26/36 of these are previously known companions and so don't need follow-up to confirm. The remaining 10 are new and unconfirmed detections; these all have very strong CCF signals and are likely to be confirmed with follow-up spectroscopy or imaging. Their inclusion does not significantly change the results.

6.1. Fitting Methodology

We use the methodology developed in Foreman-Mackey et al. (2014) to perform bayesian inference on the shape and form of the mass-ratio distribution. The log-likelihood function in this formalism is derived from modeling the survey as a draw from the inhomogeneous Poisson process with rate density $\Gamma \equiv KQ(q)P(q)$:

$$\ln \mathcal{L}(\{\mathbf{x}_k\}|\boldsymbol{\theta}) = -K \int_0^1 Q(q)P(q|\boldsymbol{\theta})dq + \sum_{k=1}^K \ln \frac{K}{N_k} \sum_{n=1}^{N_k} Q(q_k^{(n)})P(q_k^{(n)}|\boldsymbol{\theta}) \quad (9)$$

In the above equation, $\{\mathbf{x}_k\}$ denotes the data for star k , and $\boldsymbol{\theta}$ denotes the parameters for the model we are fitting. $K = 50$ is the number of stars used in the analysis, $Q(q)$ is the completeness function shown in Figure 6, and $P(q|\boldsymbol{\theta})$ is the likelihood function for the mass ratio given the model parameters. We fit the data to three distinct distributions: a histogram (P_1), a lognormal distribution (P_2), and a power law (P_3):

$$P_1(q|\boldsymbol{\theta}) = \begin{cases} \theta_1 & q \in \Delta_1 \\ \theta_2 & q \in \Delta_2 \\ \dots & \\ \theta_7 & q \in \Delta_7 \end{cases} \quad (10)$$

$$P_2(q|\boldsymbol{\theta}) = \frac{A}{q\sqrt{2\pi\sigma^2}} e^{-\frac{(\ln q - \mu)^2}{2\sigma^2}} \quad (11)$$

$$P_3(q|\boldsymbol{\theta}) = (1 - \gamma)q^{-\gamma} \quad (12)$$

The constant A in the lognormal distribution is a renormalization factor such that the distribution is only defined from $0 < q < 1$:

$$A = \frac{2}{1 - \text{erf}\left(\frac{\mu}{\sigma\sqrt{2}}\right)} \quad (13)$$

We fit all distributions via Importance Nested Sampling with the MultiNest code (Feroz et al. 2013). Following Foreman-Mackey et al. (2014), we apply a smoothing prior on the parameters $\boldsymbol{\theta}$ for the histogram model:

$$P(\boldsymbol{\theta}|\alpha, m, \tau, \epsilon) = \mathcal{N}(\boldsymbol{\theta}|m, K(\{\Delta_j\}, \alpha, \tau, \epsilon)) \quad (14)$$

$$K_{ij} = \sqrt{\left[\alpha \exp\left(-\frac{(\Delta_i - \Delta_j)^2}{2\tau^2}\right) \right]^2 + \epsilon^2 \delta_{ij}} \quad (15)$$

The smoothing prior is an 7-dimensional gaussian with mean m and covariance matrix K_{ij} , and encodes our belief that the mass-ratio distribution is a smoothly varying function while leaving enough flexibility to let the data drive the shape of the function. Since we have introduced three new hyperparameters $(\alpha, m, \tau, \epsilon)$, we must apply a prior to them and marginalize over them when estimating the bin heights. We choose log-uniform priors for α, τ , and ϵ , and a uniform prior for the mean m . The full posterior probability distribution for the histogram model is:

$$P_1(\boldsymbol{\theta}|\{\mathbf{x}_k\}) \propto \mathcal{L}_1(\{\mathbf{x}_k\}|\boldsymbol{\theta}) P(\boldsymbol{\theta}|\alpha, m, \tau, \epsilon) P(\alpha, m, \tau, \epsilon) \quad (16)$$

The lognormal distribution only has two parameters (μ, σ) , and was chosen because it has a similar shape to the histogram resulting from the first model. We use uniform priors on both μ and σ , although we note that μ is compared to $\ln q$ and so acts like a log-uniform prior. The power law has only one parameter (γ); we use a uniform prior in the fit.

6.2. Malmquist Bias Correction

We are trying to recover the intrinsic distribution from an observed sample, so we must fit the data to the probability distribution function (PDF) for mass ratio, *given that we observed the star*: $P(q|\boldsymbol{\theta}, \text{obs})$. In a volume-limited sample, this is equal to $P(q|\boldsymbol{\theta})$. However, our sample is magnitude-limited and therefore suffers from Malmquist bias. There is a higher probability for equal-mass binary systems to occur in our survey because they contribute twice the flux and are therefore more likely to fall under the magnitude limit. We can calculate the PDF for mass ratio, given that we observed the system, from Bayes' theorem:

$$P(q|\boldsymbol{\theta}, \text{obs}) = \frac{P(\text{obs}|q)P(q|\boldsymbol{\theta})}{\int_0^1 P(\text{obs}|q)P(q|\boldsymbol{\theta})dq} \quad (17)$$

We already know $P(q|\boldsymbol{\theta})$ (Equations 10 - 12). We estimate $P(\text{obs}|q)$ by simulating a very large sample of binary stars via these steps:

1. Draw random primary star masses from the Kroupa IMF (Kroupa 2002)
2. Draw a random distance for each star from a disk with infinite extent and scale height of 150 pc (the approximate scale height of the Milky Way disk for A-type stars, Binney & Merrifield 1998).
3. For each q from 0 to 1, in steps of 0.01:
 - (a) Add a companion star to each primary with the appropriate mass to make a binary system with mass ratio q .

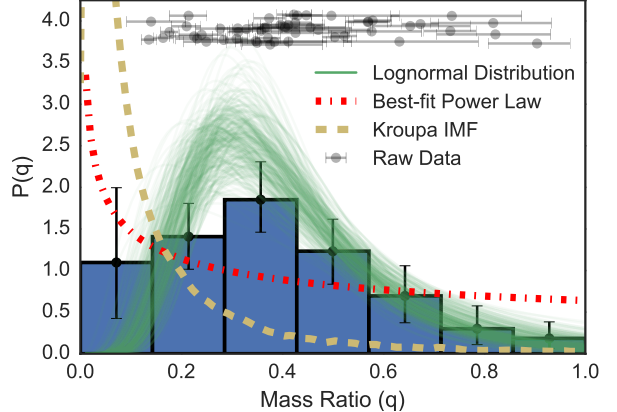


FIG. 7.— Mass-ratio distribution for our sample. The data was fit to a histogram, a lognormal distribution, and a power law. The histogram is shown in the solid blue blocks, with 1σ uncertainties marked with error bars. The variance of the lognormal fit is shown with 300 samples from the posterior probability distribution for the parameters in green. We also show the best-fit power law and the mass-ratio distribution resulting from random pairing of the Kroupa initial mass function. Finally, we display the raw mass ratio measurements with associated uncertainties in the cluster of data points near the top of the figure.

- (b) Calculate the combined absolute V-magnitude by interpolating Table 5 of Pecaut & Mamajek (2013).
- (c) Calculate apparent magnitude V from the absolute magnitude and distance.
- (d) Find fraction of stars ($f(q)$) with apparent $V < 6$
4. Fit the sampled fractions $f(q)$ to a 5th-order polynomial.

With the fitted malmquist-correction polynomial, we then substitute $P(q|\boldsymbol{\theta}, \text{obs})$ everywhere $P(q|\boldsymbol{\theta})$ appears in Equation 9.

We summarize the parameters in Table 5, and show the resulting fits in Figure 7. The 1σ uncertainties in the bin heights from the histogram model are shown as error bars, and we overplot 300 samples of the lognormal distribution fit to show the spread allowed by the data. The best-fit power law is plotted with a red dot-dashed line. We also estimate the mass-ratio distribution expected from random pairing of the Kroupa Initial Mass Function (IMF), and show the result in yellow. We estimate the distribution by drawing 100000 primary stars from the IMF with masses between $1.5 < M/M_\odot < 20$. We then draw companions from the same IMF, with the restriction that the companion has a lower mass than the primary. The result plotted in yellow in Figure 7 is a gaussian kernel density estimate of the resulting mass ratios, with a bandwidth of 0.05.

7. DISCUSSION

Previous measurements of the mass-ratio distribution find that the data is well fit by a power law. Kouwenhoven et al. (2007) compiled spectroscopic, imaging, and astrometric observations of binary stars with intermediate-mass primaries in the Scorpius OB association, and derived a power law index of -0.45 ± 0.15 . More

recently De Rosa et al. (2014) performed an adaptive optics and common proper motion search for companions to field A-type stars. They found that the distribution for companions on wide ($a > 125$ AU) orbits has a very steep power law index of $-2.3_{-0.9}^{+1.0}$, while the distribution for close (30 AU $< a < 125$ AU) companions is consistent with flat.

7.1. Model Comparison

The most striking feature of the mass-ratio distribution shown in Figure 7 is the turnover or flattening at intermediate q . The maximum of the lognormal distribution occurs at $q = 0.30 \pm 0.03$ and is an estimate of the characteristic scale.

Although the power law fit and the Kroupa IMF are visually very poor fits to the data, we formally compare the models to ensure that the different form is not an artifact of binning or simple noise. We make the comparison using the posterior odds:

$$\text{Odds} = \frac{\int_{\theta_1} P_1(q|\theta_1)P(\theta_1)}{\int_{\theta_2} P_2(q|\theta_2)P(\theta_2)} \equiv \frac{Z_1}{Z_2} \quad (18)$$

The integrals are estimated as part of the nested sampling algorithm in the MultiNest code. The odds ratio comparing the lognormal distribution to power law fit is $Z_{\text{lognormal}}/Z_{\text{power}} = 5.1 \pm 0.1 \times 10^6$, indicating a very strong preference for the lognormal distribution model. We also compare to the mass-ratio distribution expected for random pairing from the Kroupa IMF and to a uniform distribution (a special case of the power law). In these cases, there are no free parameters so the evidence integral just becomes the likelihood function (Equation 9). The corresponding odds ratios are $Z_{\text{lognormal}}/Z_{\text{IMF}} = 6.5 \pm 0.1 \times 10^{22}$ and $Z_{\text{lognormal}}/Z_{\text{uniform}} = 7.0 \pm 0.1 \times 10^6$. Both of these again demonstrate a very strong preference for the lognormal distribution.

The extreme unlikelihood of the Kroupa IMF model also indicates that our sample is not significantly biased by foreground or background contaminants. In fact, the present-day background star mass function is more bottom heavy than the initial mass function because some of the massive stars have evolved to white dwarfs or ended their lives in a supernova. The comparison to a Kroupa IMF therefore *underestimates* the likelihood of background star contamination.

7.2. Comparison to Previous Results

Our mass-ratio distribution appears to be in tension with the results of the VAST survey (De Rosa et al. 2014), which finds a nearly flat distribution for close companions. However, their subsample of close companions only includes 18 binaries, so it is possible that the different forms are just a result of small number statistics. To assess the degree of tension, we use the Anderson-Darling test (Anderson & Darling 1954) to find the probability that both their close companion subsample and our companions are drawn from the same parent distribution. We only use companions from this work with mean $\bar{q} > 0.15$ because the VAST survey subsample makes the same cut. The VAST survey also only included stars with projected separations $a < 125$ AU in their close companion subsample. Since we cannot estimate the separation from

our data, we do not make such a cut. We could make a cut using the *maximum* possible separation, set by the distance and spectrograph slit width, but doing so vastly reduces the number of detections and does not affect the result.

To account for measurement uncertainties in the mass ratios, we draw from both our mass ratio samples ($q_k^{(n)}$, see Section 6) and the VAST mass ratio values many times and compute the Anderson-Darling test statistic each time. Since De Rosa et al. (2014) do not quote uncertainties, we assume uncertainties of $\sigma_q = 0.05$ for all of their measurements. The result is $p = 0.10_{-0.04}^{+0.07}$; we cannot reject the hypothesis that both samples come from the same distribution.

7.3. Theoretical Implications

The mass-ratio distribution derived in this work has a very different form than the power law found for companions at wide separations. This is likely a result of disk interactions as the two components are accreting. The close companions that we detect may form with similar masses to their counterparts at large separations ($a \gtrsim 1000$ AU), but preferentially accrete matter from the dense primary star disk. The result would be a depletion of low mass ratio companions as they become intermediate to high mass ratio companions. The characteristic scale of ~ 0.3 that we see in Figure 7 would then be related to the disk timescale, since with enough time the preferential accretion would push all companions to $q = 1.0$.

It is also possible that some of the companions found in this work were formed from a gravitationally unstable disk (e.g. Kratter & Matzner 2006; Stamatellos & Whitworth 2011). Being a completely different formation mechanism than the way wide companions form, we would expect the initial companion mass function to differ. Such companions would undergo the same preferential accretion discussed above.

Large scale simulations are likely needed to distinguish between the two scenarios and fully interpret the results of this survey. A significant amount of work has already been put towards this end in the form of radiation hydrodynamic simulations of giant molecular clouds (Bate 2012; Krumholz et al. 2012). However, the present simulations do not generate enough stars more massive than the sun to quantitatively compare binary and multiple star statistics to observations.

8. SUMMARY

In this work, we described a binary survey of 341 bright A- and B-type stars. We used the direct spectral detection method (Gullikson et al. 2016) to find the spectral lines of 64 companions with temperatures ranging from $3600 - 16000$ K. We used the cross-correlation functions to estimate the temperature and surface gravity of most of our sample stars, and converted to mass and age by interpolating Padova stellar evolutionary tracks (Bressan et al. 2012). Likewise, we convert the companion temperature measurements to mass by using solar metallicity Dartmouth evolutionary tracks (Dotter et al. 2008).

We then use the formalism introduced in Foreman-Mackey et al. (2014), which self-consistently accounts for measurement errors, to infer the form of the mass-ratio

distribution (shown in Figure 7). Unlike most previous work, we find that a power law is a poor descriptor of the data and find that a lognormal distribution performs much better. This result, which only includes close companions since it is a spectroscopic technique, is consistent with the 18 close companions found in the VAST survey (De Rosa et al. 2014). However, this result shows much more detail due to a larger number of companions.

We interpret the mass-ratio distribution in terms of formation mechanism in Section 7.3. It is likely that the mass-ratio distribution we find is largely a result of preferential accretion onto the secondary star, which largely stops when the circumprimary or circumbinary disk dissipates.

In the effort of open and reproducible research, we have made several data products freely available to the community. All of the reduced and telluric-corrected spectra used in this study are available at <https://zenodo.org/record/46340>. Samples of the primary and companion mass and system age posterior distributions are available at <https://zenodo.org/record/48073>, as are the posterior distributions for the parameters fit in Section 6 and every cross-correlation function generated in our analysis. We additionally provide a series of python libraries and jupyter notebooks with the computer code we used for the analysis on github: <https://github.com/kgullikson88/BinaryInference>.

ACKNOWLEDGEMENTS

We would like to thank the anonymous referee for their helpful comments, which have notably improved this work. This research has made use of the SIMBAD database, operated at CDS, Strasbourg, France, and of Astropy, a community-developed core Python package for Astronomy (Astropy Collaboration, 2013). It was supported by a start-up grant to Adam Kraus as well as a University of Texas Continuing Fellowship and a Dissertation Writing Fellowship to Kevin Gullikson.

This work used the Immersion Grating Infrared Spectrograph (IGRINS) that was developed under a collaboration between the University of Texas at Austin and the Korea Astronomy and Space Science Institute (KASI) with the financial support of the US National Science Foundation under grant AST-1229522, of the University of Texas at Austin, and of the Korean GMT Project of KASI.

The Hobby-Eberly Telescope (HET) is a joint project of the University of Texas at Austin, the Pennsylvania State University, Stanford University, Ludwig-Maximilians-Universität München, and Georg-August-Universität Göttingen. The HET is named in honor of its principal benefactors, William P. Hobby and Robert E. Eberly.

Based on observations at Cerro Tololo Inter-American Observatory, National Optical Astronomy Observatory (NOAO Prop. IDs: 13A-0139, 13B-0112, 2014A-0260, 14A-0260, 15A-0245; PI: Kevin Gullikson), which is operated by the Association of Universities for Research in Astronomy (AURA) under a cooperative agreement with the National Science Foundation.

TABLE 1
 SAMPLE PROPERTIES

star	SpT	RA	DEC	V	parallax (mas)	T_{eff} (K)	$\log g$ (cgs)	Mass (M_{\odot})	Age (Myr)	Ref
HIP 813	B9Vn	00:10:02.20	+11:08:44.93	5.537	10.68	12516 ± 426	4.3 ± 0.14	3.1 ^{+0.18} _{-0.17}	85 ⁺⁵⁶ ₋₅₂	1
HIP 1191	B8.5V	00:14:54.52	-09:34:10.45	5.757	9.63	12000 ± 1000	4.5 ± 0.25	2.8 ^{+0.41} _{-0.37}	23 ⁺⁶³ ₋₁₆	2
HIP 1366	A2V	00:17:05.50	+38:40:53.89	4.610	10.56	9371 ± 319	4.0 ± 0.14	2.2 ^{+0.18} _{-0.16}	464 ⁺⁸³ ₋₁₁₉	1
HIP 1647	B9V	00:20:39.04	-69:37:29.68	5.498	10.25	11393 ± 387	4.0 ± 0.14	2.8 ^{+0.21} _{-0.18}	206 ⁺⁴⁸ ₋₇₉	1
HIP 2381	A3V	00:30:22.65	-23:47:15.65	5.190	18.83	8364 ± 284	4.0 ± 0.14	1.9 ^{+0.16} _{-0.13}	715 ⁺¹³⁵ ₋₁₈₃	1
HIP 2505	B8Vn	00:31:46.36	+54:31:20.23	4.732	8.64	12000 ± 1000	4.0 ± 0.25	2.9 ^{+0.45} _{-0.40}	58 ⁺¹⁰⁴ ₋₄₈	2
HIP 2548	B9.5V	00:32:23.78	+06:57:19.66	5.698	12.35	11864 ± 403	4.4 ± 0.14	2.8 ^{+0.15} _{-0.15}	77 ⁺⁶⁹ ₋₅₁	1
HIP 3300	B2V	00:42:03.90	+50:30:45.09	4.810	2.28	18000 ± 1000	4.0 ± 0.25	5.7 ^{+0.67} _{-0.63}	19 ⁺¹⁹ ₋₁₃	2
HIP 3478	B5V	00:44:26.19	+47:51:50.34	5.646	5.23	18000 ± 1000	4.5 ± 0.25	5.4 ^{+0.60} _{-0.57}	11 ⁺¹⁴ ₋₅	2
HIP 5131	A1Vn	01:05:40.96	+21:28:23.45	5.317	11.86	11956 ± 406	4.4 ± 0.14	2.8 ^{+0.16} _{-0.14}	69 ⁺⁶⁵ ₋₄₅	1
HIP 5132	A0Vn	01:05:41.71	+21:27:55.60	5.532	11.64	12053 ± 410	4.4 ± 0.14	2.9 ^{+0.16} _{-0.14}	64 ⁺⁶¹ ₋₄₂	1
HIP 5310	A3V	01:07:57.16	+20:44:20.83	5.569	21.14	8611 ± 293	4.4 ± 0.14	1.8 ^{+0.10} _{-0.08}	307 ⁺²²⁸ ₋₁₉₆	1
HIP 5361	B8V	01:08:33.47	+58:15:48.41	5.773	5.41	14000 ± 1000	4.5 ± 0.25	3.6 ^{+0.49} _{-0.43}	18 ⁺³⁶ ₋₁₁	2
HIP 5518	A0Vnn	01:10:39.32	+68:46:43.04	5.318	11.78	11894 ± 404	4.1 ± 0.14	3.0 ^{+0.21} _{-0.19}	172 ⁺⁴⁰ ₋₇₂	1
HIP 5626	A3V	01:12:16.82	+79:40:26.27	5.600	12.07	10342 ± 352	4.2 ± 0.14	2.4 ^{+0.15} _{-0.14}	218 ⁺¹⁰² ₋₁₂₇	1
HIP 7345	A1V	01:34:37.78	-15:40:34.90	5.619	16.84	10007 ± 340	4.4 ± 0.14	2.2 ^{+0.12} _{-0.11}	156 ⁺¹³⁰ ₋₁₀₀	1
HIP 8016	B9V	01:42:55.86	+70:37:21.09	5.177	11.75	10000 ± 500	4.0 ± 0.25	2.3 ^{+0.25} _{-0.21}	67 ⁺¹⁸⁸ ₋₅₇	2
HIP 8704	B1.5V	01:51:59.32	+55:08:50.58	5.520	2.52	22000 ± 1000	4.5 ± 0.25	7.8 ^{+0.74} _{-0.70}	8 ⁺⁶ ₋₃	2
HR 545	B9V	01:53:31.77	+19:17:46.27	4.700	...	10000 ± 500	4.5 ± 0.25	2.2 ^{+0.21} _{-0.20}	34 ⁺¹⁰⁶ ₋₂₇	2
HIP 9312	A0Vn	01:59:38.04	+64:37:17.76	5.283	13.28	11913 ± 405	4.1 ± 0.14	2.8 ^{+0.13} _{-0.11}	77 ⁺⁶⁵ ₋₅₀	1
HIP 9564	A1Vn	02:02:52.48	+64:54:05.27	5.999	11.92	11266 ± 383	4.3 ± 0.14	2.7 ^{+0.15} _{-0.12}	149 ⁺⁷⁴ ₋₈₈	1
HR 604	B8V	02:03:54.72	+42:19:51.41	5.820	...	10000 ± 500	3.5 ± 0.25	2.8 ^{+0.46} _{-0.42}	281 ⁺⁸² ₋₁₁₇	2
HIP 10320	B9V	02:12:54.47	-30:43:25.77	5.261	10.18	11745 ± 399	3.7 ± 0.14	3.1 ^{+0.23} _{-0.19}	205 ⁺²² ₋₄₃	1
HIP 10670	A1Vnn	02:17:18.87	+33:50:49.90	4.000	29.04	10772 ± 366	4.2 ± 0.14	2.6 ^{+0.16} _{-0.13}	230 ⁺⁶³ ₋₁₀₉	1
HIP 10732	A1Vn	02:18:07.54	+19:54:04.19	5.575	7.29	9500 ± 1000	4.0 ± 0.25	2.1 ^{+0.37} _{-0.31}	107 ⁺²⁸⁶ ₋₉₃	2
HIP 11345	A0V	02:25:57.01	-12:17:25.71	4.869	7.15	10000 ± 500	4.0 ± 0.25	2.3 ^{+0.25} _{-0.22}	72 ⁺²⁰⁶ ₋₆₀	2
HIP 12332	A7V	02:38:48.99	+21:57:41.06	5.454	9.68	8000 ± 500	3.5 ± 0.25	2.0 ^{+0.40} _{-0.33}	621 ⁺²⁶⁹ ₋₂₆₈	2
HIP 12706	A2Vn	02:43:18.04	+03:14:08.94	3.470	40.97	8551 ± 291	4.3 ± 0.14	1.9 ^{+0.15} _{-0.13}	647 ⁺¹⁰⁴ ₋₁₈₄	1
HIP 12719	B3V	02:43:27.11	+27:42:25.72	4.670	9.51	18000 ± 1000	4.5 ± 0.25	5.4 ^{+0.62} _{-0.57}	11 ⁺¹⁴ ₋₅	2
HIP 12803	B9Vn	02:44:32.97	+15:18:42.71	5.776	5.49	12000 ± 1000	4.5 ± 0.25	2.8 ^{+0.39} _{-0.36}	25 ⁺⁶³ ₋₁₇	2
HIP 13165	B6V	02:49:17.56	+17:27:51.52	5.314	4.18	16000 ± 1000	4.5 ± 0.25	4.4 ^{+0.59} _{-0.51}	13 ⁺²² ₋₇	2
HIP 13202	A0V	02:49:54.18	-27:56:31.14	5.389	7.11	9000 ± 500	3.5 ± 0.25	2.4 ^{+0.44} _{-0.38}	401 ⁺¹³⁸ ₋₁₇₀	2
HIP 13209	B8Vn	02:49:59.03	+27:15:37.83	3.606	19.69	13316 ± 453	4.1 ± 0.14	3.3 ^{+0.15} _{-0.13}	45 ⁺⁴³ ₋₃₀	1
HIP 13327	B7V	02:51:29.59	+15:04:55.45	5.514	6.60	14000 ± 1000	4.0 ± 0.25	3.8 ^{+0.55} _{-0.46}	36 ⁺⁵⁷ ₋₂₇	2
HIP 13717	A3V	02:56:37.42	-03:42:44.35	5.160	17.49	8612 ± 293	4.0 ± 0.14	1.9 ^{+0.13} _{-0.11}	571 ⁺¹³⁸ ₋₂₅₅	1
HIP 13879	A2Vn	02:58:45.67	+39:39:45.81	4.700	10.53	9298 ± 316	3.5 ± 0.14	2.1 ^{+0.12} _{-0.09}	340 ⁺¹⁴¹ ₋₁₉₃	1
HIP 14043	B7V	03:00:52.21	+52:21:06.22	5.253	7.11	14000 ± 1000	4.5 ± 0.25	3.6 ^{+0.48} _{-0.45}	17 ⁺³³ ₋₁₀	2
HIP 14293	A5V	03:04:16.52	-07:36:03.08	5.300	24.06	8039 ± 273	4.2 ± 0.14	1.8 ^{+0.14} _{-0.10}	782 ⁺¹⁶⁶ ₋₂₉₁	1
HIP 14764	B8V	03:10:38.79	+11:52:21.44	5.965	7.33	12000 ± 1000	4.0 ± 0.25	2.9 ^{+0.47} _{-0.40}	54 ⁺¹⁰³ ₋₄₄	2
HIP 14862	A2Vnn	03:11:56.27	+74:23:37.17	4.840	19.72	8875 ± 1000	4.2 ± 0.25	1.8 ^{+0.32} _{-0.29}	71 ⁺³¹⁷ ₋₆₀	2
HIP 15110	A1V	03:14:54.10	+21:02:40.01	4.880	12.44	9902 ± 337	4.0 ± 0.14	2.4 ^{+0.18} _{-0.15}	375 ⁺⁵² ₋₁₀₄	1
HIP 15338	B8V	03:17:47.35	+44:01:30.08	5.478	4.46	12000 ± 1000	3.5 ± 0.25	3.5 ^{+0.65} _{-0.59}	155 ⁺⁶⁸ ₋₅₉	2
HIP 15404	B3V	03:18:37.74	+50:13:19.83	5.158	5.12	20000 ± 1000	4.5 ± 0.25	6.5 ^{+0.68} _{-0.64}	9 ⁺⁹ ₋₄	2
HIP 15444	B5V	03:19:07.64	+50:05:41.88	5.036	5.82	18000 ± 1000	4.5 ± 0.25	5.5 ^{+0.60} _{-0.60}	11 ⁺¹⁴ ₋₆	2
HIP 16210	B6Vn	03:28:52.33	+49:50:54.17	5.578	6.22
HIP 16244	B3V	03:29:22.05	+49:30:32.21	4.678	6.05	18000 ± 1000	4.5 ± 0.25	5.4 ^{+0.61} _{-0.57}	11 ⁺¹⁴ ₋₅	2
HIP 16285	A5V	03:29:55.15	-42:38:03.32	5.768	15.28	7884 ± 268	3.9 ± 0.14	1.7 ^{+0.13} _{-0.09}	841 ⁺¹⁸³ ₋₃₃₅	1
HIP 16322	A0Vn	03:30:24.47	+11:20:11.19	5.125	9.03	10000 ± 500	4.0 ± 0.25	2.3 ^{+0.26} _{-0.22}	80 ⁺²⁰⁰ ₋₆₉	2
HIP 16340	B8V	03:30:36.95	+48:06:12.95	5.820	3.65	12000 ± 1000	4.0 ± 0.25	2.9 ^{+0.48} _{-0.40}	54 ⁺¹⁰⁷ ₋₄₄	2
HIP 16599	A3V	03:33:39.06	+54:58:29.49	5.981	13.44	8383 ± 285	4.0 ± 0.14	2.0 ^{+0.19} _{-0.15}	737 ⁺¹⁰² ₋₁₀₂	1
HIP 16611	B9V	03:33:47.28	-21:37:58.38	4.300	11.12	12514 ± 425	4.0 ± 0.14	3.3 ^{+0.24} _{-0.20}	157 ⁺²³ ₋₄₅	1
HIP 17457	B7IV	03:44:30.51	-01:09:47.14	5.250	4.98	14000 ± 1000	4.5 ± 0.25	3.6 ^{+0.47} _{-0.44}	17 ⁺³⁶ ₋₁₀	2
HIP 17527	B8V	03:45:09.74	+24:50:21.34	5.640	7.97	14000 ± 1000	4.5 ± 0.25	3.6 ^{+0.47} _{-0.44}	18 ⁺³⁴ ₋₁₁	2
HIP 17563	B3V	03:45:40.44	+06:02:59.97	5.332	6.11	18000 ± 1000	4.5 ± 0.25	5.4 ^{+0.64} _{-0.57}	11 ⁺¹⁴ ₋₅	2
HIP 18141	B8V	03:52:41.66	-05:21:40.54	5.476	5.57	14000 ± 1000	4.5 ± 0.25	3.6 ^{+0.47} _{-0.43}	18 ⁺³⁵ ₋₁₂	2
HIP 18396	B6V	03:55:58.17	+47:52:17.12	5.379	4.47	16000 ± 1000	4.5 ± 0.25	4.5 ^{+0.54} _{-0.50}	14 ⁺²¹ ₋₈	2
HIP 18788	B5V	04:01:32.05	-01:32:58.78	5.280	7.88	16000 ± 1000	4.5 ± 0.25	4.5 ^{+0.60} _{-0.57}	13 ⁺²² ₋₇	2
HIP 18805	B5V	04:01:46.14	+09:59:52.84	5.676	5.71	18000 ± 1000	4.5 ± 0.25	5.4 ^{+0.57} _{-0.57}	10 ⁺¹⁴ ₋₅	2

TABLE 1 — *Continued*

star	SpT	RA	DEC	V	parallax (mas)	T_{eff} (K)	$\log g$ (cgs)	Mass (M_{\odot})	Age (Myr)	Ref
HIP 19799	B9Vn	04:14:36.23	+10:00:41.05	5.208	8.34	10000 ± 500	4.5 ± 0.25	$2.2^{+0.21}_{-0.19}$	34^{+116}_{-26}	2
HIP 19949	A2Vn	04:16:43.09	+53:36:42.47	5.200	9.98	9825 ± 334	3.8 ± 0.14	$2.2^{+0.11}_{-0.10}$	197^{+140}_{-122}	1
HIP 19968	B7V	04:16:53.56	+61:50:59.97	5.700	7.31	16000 ± 1000	4.5 ± 0.25	$4.5^{+0.53}_{-0.51}$	13^{+21}_{-13}	2
HIP 20264	A0V	04:20:39.01	-20:38:22.64	5.380	6.86	10000 ± 500	4.0 ± 0.25	$2.3^{+0.25}_{-0.21}$	77^{+207}_{-65}	2
HIP 20380	A3V	04:21:51.81	+56:30:22.74	5.920	10.31	8738 ± 297	3.9 ± 0.14	$1.9^{+0.10}_{-0.08}$	338^{+206}_{-209}	1
HIP 20430	B9Vnn	04:22:34.94	+25:37:45.54	5.376	11.20	11981 ± 407	4.2 ± 0.14	$3.2^{+0.28}_{-0.23}$	195^{+23}_{-27}	1
HIP 20507	A2V	04:23:40.85	-03:44:43.68	5.171	15.60	8793 ± 299	4.0 ± 0.14	$1.9^{+0.10}_{-0.08}$	340^{+200}_{-210}	1
HIP 20579	B8V	04:24:29.16	+34:07:50.73	5.722	7.28	14000 ± 1000	4.5 ± 0.25	$3.6^{+0.46}_{-0.46}$	17^{+32}_{-10}	2
HIP 20789	B7V	04:27:17.45	+22:59:46.80	5.515	8.63	14000 ± 1000	4.0 ± 0.25	$3.7^{+0.53}_{-0.47}$	38^{+55}_{-28}	2
HIP 21589	A6V	04:38:09.46	+12:30:39.01	4.270	21.24	8591 ± 292	3.9 ± 0.14	$1.8^{+0.09}_{-0.07}$	300^{+231}_{-193}	1
HIP 21683	A5Vn	04:39:16.50	+15:55:04.70	4.675	20.97	8165 ± 278	4.0 ± 0.14	$1.7^{+0.07}_{-0.06}$	318^{+266}_{-211}	1
HIP 21819	A2V	04:41:19.76	+28:36:53.98	5.726	8.55	9000 ± 500	3.5 ± 0.25	$2.4^{+0.41}_{-0.37}$	411^{+135}_{-158}	2
HIP 21928	A1Vn	04:42:54.33	+43:21:54.53	5.301	13.52	10734 ± 365	4.0 ± 0.14	$2.6^{+0.16}_{-0.13}$	242^{+59}_{-108}	1
HIP 22028	A1V	04:44:07.98	-18:39:59.71	5.527	10.66	10118 ± 344	4.0 ± 0.14	$2.3^{+0.14}_{-0.11}$	246^{+105}_{-135}	1
HIP 22509	A1Vn	04:50:36.72	+08:54:00.65	4.350	14.53	9784 ± 333	2.7 ± 0.14	$2.2^{+0.11}_{-0.10}$	205^{+141}_{-129}	1
HIP 22833	A3V	04:54:46.90	+11:25:33.63	5.186	14.29	8278 ± 281	3.9 ± 0.14	$1.8^{+0.12}_{-0.09}$	645^{+165}_{-304}	1
HIP 22840	B5V	04:54:50.71	+00:28:01.81	5.975	4.50	16000 ± 1000	4.0 ± 0.25	$4.7^{+0.61}_{-0.55}$	27^{+32}_{-18}	2
HIP 22913	B9V	04:55:50.15	+15:02:25.00	5.785	8.97	12000 ± 1000	3.5 ± 0.25	$3.5^{+0.67}_{-0.57}$	155^{+68}_{-64}	2
HIP 22958	B6V	04:56:24.19	-05:10:16.87	5.490	4.40	16000 ± 1000	4.5 ± 0.25	$4.5^{+0.52}_{-0.53}$	13^{+20}_{-64}	2
HIP 23362	B9V	05:01:25.58	-20:03:06.91	4.894	16.48	12450 ± 423	4.3 ± 0.14	$3.2^{+0.21}_{-0.16}$	147^{+28}_{-59}	1
HIP 23916	B8V	05:08:20.19	-08:39:55.17	5.780	4.79
HIP 24244	B7.5Vn	05:12:17.90	-11:52:09.19	4.450	14.07	13781 ± 469	4.2 ± 0.14	$3.9^{+0.29}_{-0.23}$	114^{+11}_{-23}	1
HIP 24327	B7V	05:13:13.88	-12:56:28.65	4.421	4.48	14000 ± 1000	4.5 ± 0.25	$3.6^{+0.47}_{-0.44}$	18^{+35}_{-11}	2
HIP 24505	B9V	05:15:24.37	-26:56:36.63	5.040	11.73	11748 ± 399	4.2 ± 0.14	$2.9^{+0.16}_{-0.14}$	152^{+53}_{-80}	1
HIP 24902	A3V	05:20:14.67	+41:05:10.35	5.468	11.77	8275 ± 281	4.0 ± 0.14	$1.8^{+0.09}_{-0.08}$	457^{+261}_{-281}	1
ADS 3962 AB	B1Vn	05:22:50.30	+03:32:52.00	4.990
HIP 25143	A3V	05:22:50.31	+41:01:45.33	5.545	11.15	8101 ± 275	3.8 ± 0.14	$1.7^{+0.06}_{-0.06}$	231^{+250}_{-156}	1
HIP 25280	A0V	05:24:28.49	-16:58:32.81	5.644	14.65	10398 ± 354	4.4 ± 0.14	$2.4^{+0.13}_{-0.11}$	199^{+101}_{-115}	1
HIP 25555	B9.5Vn	05:27:45.61	+15:52:26.58	5.512	7.69	10000 ± 500	3.5 ± 0.25	$2.8^{+0.45}_{-0.43}$	283^{+79}_{-104}	2
HIP 25608	A1V	05:28:15.34	-37:13:50.75	5.562	11.39	9960 ± 339	4.1 ± 0.14	$2.3^{+0.15}_{-0.12}$	311^{+83}_{-149}	1
HIP 25695	B9Vn	05:29:16.50	+25:09:00.78	5.480	7.67	12000 ± 1000	4.5 ± 0.25	$2.8^{+0.43}_{-0.37}$	24^{+63}_{-17}	2
HIP 25790	A3Vn	05:30:26.16	+15:21:37.61	5.940	12.89	8397 ± 286	3.9 ± 0.14	$1.8^{+0.08}_{-0.07}$	329^{+250}_{-212}	1
HIP 25813	B5V	05:30:47.05	+05:56:53.29	4.200	10.77	15603 ± 531	4.4 ± 0.14	$4.7^{+0.35}_{-0.28}$	71^{+8}_{-16}	1
HIP 26063	B1V	05:33:31.45	-01:09:21.87	5.340	2.22
HIP 26093	B3V	05:33:54.28	+14:18:20.08	5.588	7.31	20000 ± 1000	4.5 ± 0.25	$6.6^{+0.66}_{-0.64}$	9^{+9}_{-4}	2
HIP 26126	A2V	05:34:16.77	+03:46:00.82	5.332	11.82	9542 ± 324	3.9 ± 0.14	$2.1^{+0.06}_{-0.07}$	177^{+150}_{-115}	1
HIP 26563	A4Vn	05:38:53.08	-07:12:46.18	4.800	22.42	8416 ± 286	4.1 ± 0.14	$1.8^{+0.08}_{-0.07}$	344^{+256}_{-218}	1
HIP 27100	A7V	05:44:46.38	-65:44:07.90	4.360	21.80	7828 ± 266	3.9 ± 0.14	$1.8^{+0.18}_{-0.15}$	965^{+153}_{-148}	1
HIP 27321	A6V	05:47:17.09	-51:03:59.44	3.860	51.44	8300 ± 282	4.4 ± 0.14	$1.8^{+0.11}_{-0.09}$	528^{+235}_{-300}	1
HIP 27713	A2Vn	05:52:07.73	-09:02:30.84	5.964	10.11	8474 ± 288	3.9 ± 0.14	$1.8^{+0.09}_{-0.07}$	383^{+238}_{-240}	1
HIP 28691	B5V	06:03:27.37	+19:41:26.02	5.135	4.54	14000 ± 1000	4.0 ± 0.25	$3.8^{+0.54}_{-0.48}$	36^{+55}_{-27}	2
HIP 28756	B2.5V	06:04:20.27	-32:10:20.74	5.631	3.24	20000 ± 1000	4.0 ± 0.25	$6.9^{+0.75}_{-0.68}$	14^{+13}_{-8}	2
HIP 28910	A0V	06:06:09.32	-14:56:06.92	4.669	18.88	10453 ± 355	4.1 ± 0.14	$2.4^{+0.14}_{-0.12}$	252^{+80}_{-122}	1
HIP 29150	A0V	06:08:57.87	-22:25:38.68	5.482	13.24	11283 ± 384	4.2 ± 0.14	$2.6^{+0.12}_{-0.11}$	112^{+82}_{-71}	1
HIP 29151	A3Vn	06:08:57.90	+02:29:58.89	5.730	4.98	9000 ± 500	3.5 ± 0.25	$2.4^{+0.43}_{-0.37}$	406^{+141}_{-177}	2
HIP 29735	B9V	06:15:44.89	-13:43:06.29	4.998	8.00	10000 ± 500	3.5 ± 0.25	$2.8^{+0.48}_{-0.41}$	281^{+84}_{-105}	2
HIP 29997	A0Vn	06:18:50.78	+69:19:11.23	4.762	18.64	10834 ± 368	4.2 ± 0.14	$2.5^{+0.12}_{-0.10}$	119^{+95}_{-77}	1
HIP 30069	B9V	06:19:40.96	-34:23:47.73	5.750	8.00	12000 ± 1000	4.5 ± 0.25	$2.8^{+0.42}_{-0.38}$	25^{+62}_{-18}	2
HIP 30073	B2V	06:19:42.7989	-07:49:22.473	5.246	3.74	22000 ± 1000	4.5 ± 0.25	$7.8^{+0.71}_{-0.71}$	8^{+6}_{-3}	2
HIP 30666	A3Vn	06:26:39.59	-01:30:26.41	5.874	13.80	10520 ± 358	4.2 ± 0.14	$2.6^{+0.20}_{-0.16}$	304^{+37}_{-72}	1
HIP 30788	B4V	06:28:10.21	-32:34:48.25	4.480	7.70	18000 ± 1000	4.5 ± 0.25	$5.4^{+0.59}_{-0.57}$	11^{+13}_{-6}	2
HIP 31278	B5Vn	06:33:37.92	-01:13:12.55	5.083	5.89	16000 ± 1000	4.0 ± 0.25	$4.7^{+0.61}_{-0.56}$	26^{+31}_{-18}	2
HIP 31362	B8V	06:34:35.33	-32:42:58.51	5.610	6.20	12000 ± 1000	4.5 ± 0.25	$2.8^{+0.41}_{-0.37}$	24^{+62}_{-17}	2
HIP 31434	A0Vnn	06:35:12.06	+28:01:20.32	5.266	8.82	10000 ± 500	3.5 ± 0.25	$2.7^{+0.46}_{-0.41}$	281^{+83}_{-131}	2
HIP 32474	B9.5V	06:46:39.02	-10:06:26.50	5.653	6.04	10000 ± 500	3.5 ± 0.25	$2.8^{+0.47}_{-0.43}$	281^{+85}_{-117}	2
HIP 32607	A8V	06:48:11.46	-61:56:29.00	3.300	33.78	7770 ± 264	3.8 ± 0.14	$1.6^{+0.07}_{-0.06}$	519^{+344}_{-333}	1
HIP 33372	B8Vn	06:56:25.83	+09:57:23.67	5.905	7.18	14000 ± 1000	4.5 ± 0.25	$3.6^{+0.47}_{-0.46}$	18^{+37}_{-11}	2
HIP 34769	A2V	07:11:51.86	-00:29:33.96	4.150	8.49	9000 ± 500	3.5 ± 0.25	$2.4^{+0.43}_{-0.38}$	405^{+135}_{-207}	2
HIP 35180	A1V	07:16:14.55	-15:35:08.49	5.454	12.12	9562 ± 325	4.1 ± 0.14	$2.1^{+0.12}_{-0.09}$	267^{+139}_{-158}	1

TABLE 1 — *Continued*

star	SpT	RA	DEC	V	parallax (mas)	T_{eff} (K)	$\log g$ (cgs)	Mass (M_{\odot})	Age (Myr)	Ref
HIP 35341	A5Vn	07:18:02.22	+40:53:00.22	5.870	11.73	8014 ± 272	3.9 ± 0.14	$1.7^{+0.07}_{-0.06}$	357^{+293}_{-237}	1
HIP 36393	A4V	07:29:20.44	+28:07:05.79	5.072	18.51	9184 ± 312	4.1 ± 0.14	$2.1^{+0.15}_{-0.13}$	431^{+128}_{-200}	1
HIP 36760	A1Vn	07:33:36.48	+15:49:35.98	5.269	7.70	9000 ± 500	3.7 ± 0.25	$2.1^{+0.40}_{-0.26}$	351^{+173}_{-318}	2
HIP 36812	A0Vnn	07:34:15.89	+03:22:18.19	5.830	5.67	9500 ± 1000	4.0 ± 0.25	$2.1^{+0.40}_{-0.31}$	108^{+273}_{-95}	2
HIP 36917	B7V	07:35:22.89	-28:22:09.57	4.630	14.72	13926 ± 473	4.3 ± 0.14	$3.7^{+0.17}_{-0.15}$	62^{+35}_{-37}	1
HIP 37297	B2.5V	07:39:27.34	-38:18:28.88	4.840	5.87	20000 ± 1000	4.5 ± 0.25	$6.6^{+0.67}_{-0.62}$	9^{+9}_{-4}	2
HIP 37322	B5V	07:39:43.81	-38:08:21.44	5.664	5.70	16000 ± 1000	4.5 ± 0.25	$4.5^{+0.50}_{-0.50}$	13^{+22}_{-7}	2
HIP 37450	B5V	07:41:15.81	-38:32:00.72	5.410	5.50	16000 ± 1000	4.5 ± 0.25	$4.4^{+0.53}_{-0.48}$	13^{+22}_{-8}	2
HIP 38538	A3V	07:53:29.81	+26:45:56.82	4.977	14.66	8551 ± 291	4.0 ± 0.14	$1.9^{+0.15}_{-0.12}$	637^{+111}_{-199}	1
HIP 38593	B2V	07:54:11.01	-35:52:38.23	5.462	4.81	22000 ± 1000	4.5 ± 0.25	$7.8^{+0.77}_{-0.68}$	8^{+6}_{-3}	2
HIP 38846	B2.5V	07:56:57.80	-43:30:01.48	5.340	2.08	22000 ± 1000	4.5 ± 0.25	$7.8^{+0.75}_{-0.72}$	8^{+6}_{-3}	2
HIP 39095	A1V	07:59:52.05	-18:23:57.23	4.610	13.52	8872 ± 302	3.4 ± 0.14	$2.1^{+0.18}_{-0.15}$	593^{+74}_{-85}	1
HIP 39236	B9.5Vn	08:01:30.29	+16:27:19.12	5.990	6.04	10000 ± 500	4.5 ± 0.25	$2.2^{+0.21}_{-0.19}$	36^{+119}_{-27}	2
HIP 39567	A1V	08:05:04.49	+13:07:05.58	5.146	15.20	10352 ± 352	4.3 ± 0.14	$2.4^{+0.12}_{-0.10}$	178^{+110}_{-109}	1
HIP 39847	A2V	08:08:27.45	+51:30:24.01	4.802	13.04	10014 ± 340	4.0 ± 0.14	$2.2^{+0.14}_{-0.12}$	190^{+127}_{-116}	1
HIP 39906	B5V	08:09:01.64	-19:14:42.05	4.390	7.01	18000 ± 1000	4.5 ± 0.25	$5.4^{+0.63}_{-0.54}$	11^{+15}_{-5}	2
HIP 40429	A2V	08:15:15.92	-62:54:56.32	5.160	12.90	8725 ± 297	3.9 ± 0.14	$2.1^{+0.20}_{-0.17}$	635^{+88}_{-88}	1
HIP 40706	A8V	08:18:33.31	-36:39:33.44	4.400	34.93	7986 ± 272	4.3 ± 0.14	$1.7^{+0.08}_{-0.06}$	540^{+282}_{-330}	1
HIP 40881	B9.5V	08:20:32.14	+24:01:20.32	5.930	7.13	9500 ± 1000	4.0 ± 0.25	$2.1^{+0.39}_{-0.32}$	105^{+287}_{-93}	2
HIP 41039	B1V	08:22:31.69	-48:29:25.36	4.820	1.90
HIP 41307	A0Va	08:25:39.63	-03:54:23.12	3.900	26.66	10281 ± 350	4.2 ± 0.14	$2.3^{+0.12}_{-0.10}$	201^{+109}_{-120}	1
HIP 42090	A2Vnn	08:34:43.88	+36:25:10.63	5.755	9.19	9000 ± 1000	4.0 ± 0.25	$1.9^{+0.36}_{-0.31}$	133^{+379}_{-119}	2
HIP 42129	B3V	08:35:15.56	-58:13:29.05	5.241	3.64	18000 ± 1000	4.5 ± 0.25	$5.4^{+0.61}_{-0.56}$	11^{+14}_{-5}	2
HIP 42313	A0Vnn	08:37:39.37	+05:42:13.61	4.137	20.34	11055 ± 376	4.0 ± 0.14	$2.9^{+0.23}_{-0.19}$	260^{+29}_{-44}	1
HIP 42334	A0V	08:37:52.15	-26:15:18.01	5.270	14.07	11614 ± 395	4.3 ± 0.14	$2.7^{+0.12}_{-0.10}$	79^{+71}_{-51}	1
HIP 43142	A3V	08:47:14.99	-01:53:49.31	5.279	8.12	9000 ± 500	4.0 ± 0.25	$2.0^{+0.21}_{-0.18}$	94^{+314}_{-83}	2
HIP 44127	A7V	08:59:12.45	+48:02:30.57	3.140	68.92	8233 ± 280	4.4 ± 0.14	$1.7^{+0.09}_{-0.07}$	474^{+257}_{-294}	1
HIP 44307	A2V	09:01:24.13	+32:15:08.26	5.870	6.99	8500 ± 1000	4.0 ± 0.25	$1.7^{+0.33}_{-0.28}$	162^{+257}_{-148}	2
HIP 45336	B9.5V	09:14:21.86	+02:18:51.34	3.880	28.74	10826 ± 368	4.2 ± 0.14	$2.5^{+0.12}_{-0.10}$	111^{+95}_{-71}	1
HIP 45344	B4V	09:14:24.48	-43:13:38.97	5.250	5.33	18000 ± 1000	4.5 ± 0.25	$5.4^{+0.62}_{-0.57}$	11^{+14}_{-5}	2
HIP 45688	A1V	09:18:50.64	+36:48:09.33	3.820	26.13	8862 ± 301	3.9 ± 0.14	$1.9^{+0.08}_{-0.07}$	255^{+202}_{-160}	1
HIP 46225	A4V	09:25:27.23	-61:57:01.72	5.781	12.92	8577 ± 292	4.0 ± 0.14	$1.8^{+0.10}_{-0.07}$	418^{+206}_{-252}	1
HIP 46283	B6V	09:26:17.96	-53:22:44.07	5.088	7.60	16000 ± 1000	4.5 ± 0.25	$4.5^{+0.54}_{-0.50}$	13^{+20}_{-8}	2
HIP 46897	B9.5V	09:33:26.05	-22:51:49.99	5.911	12.46	10075 ± 343	4.2 ± 0.14	$2.3^{+0.16}_{-0.13}$	286^{+93}_{-140}	1
HIP 47006	A0Vn	09:34:49.43	+52:03:05.32	4.479	12.44	9757 ± 332	3.9 ± 0.14	$2.1^{+0.10}_{-0.08}$	181^{+138}_{-114}	1
HIP 47175	A7V	09:36:49.54	-49:21:18.09	4.350	30.94	8331 ± 283	4.3 ± 0.14	$1.8^{+0.11}_{-0.09}$	453^{+256}_{-278}	1
HIP 50303	A0Vn	10:16:14.43	+29:18:37.81	5.490	12.51	10377 ± 353	4.1 ± 0.14	$2.4^{+0.13}_{-0.11}$	204^{+103}_{-116}	1
HIP 50860	A6V	10:23:06.33	+33:54:29.31	5.900	13.46	8327 ± 283	4.1 ± 0.14	$1.8^{+0.11}_{-0.09}$	591^{+183}_{-303}	1
HIP 51362	B9.5V	10:29:28.70	-02:44:20.69	5.180	10.13	10899 ± 371	4.0 ± 0.14	$2.6^{+0.14}_{-0.12}$	182^{+81}_{-101}	1
HIP 51685	A2Vn	10:33:30.91	+34:59:19.30	5.580	4.77	9000 ± 500	3.5 ± 0.25	$2.4^{+0.42}_{-0.38}$	406^{+134}_{-172}	2
HIP 52422	A4Vn	10:43:01.88	+26:19:32.09	5.517	20.67	8170 ± 278	4.3 ± 0.14	$1.7^{+0.08}_{-0.06}$	432^{+278}_{-278}	1
HIP 52457	A3Vn	10:43:24.96	+23:11:18.25	5.075	14.23	9902 ± 337	4.0 ± 0.14	$2.2^{+0.12}_{-0.10}$	228^{+126}_{-137}	1
HIP 52638	A1Vn	10:45:51.89	+30:40:56.33	5.349	8.53	10000 ± 500	4.0 ± 0.25	$2.3^{+0.25}_{-0.21}$	69^{+199}_{-59}	2
HIP 52678	B6Vnn	10:46:16.56	-64:30:52.41	5.340	6.85	16000 ± 1000	4.5 ± 0.25	$4.4^{+0.55}_{-0.48}$	13^{+20}_{-7}	2
HIP 52736	B2.5Vn	10:46:51.22	-64:23:00.50	4.850	6.79	20000 ± 1000	4.5 ± 0.25	$6.5^{+0.66}_{-0.62}$	9^{+9}_{-4}	2
HIP 52911	A2V	10:49:15.43	+10:32:42.73	5.314	8.57	9000 ± 500	3.5 ± 0.25	$2.4^{+0.44}_{-0.37}$	406^{+138}_{-172}	2
HR 4259	A1V	10:55:36.80	+24:44:59.00	4.500	...	9000 ± 500	3.5 ± 0.25	$2.4^{+0.44}_{-0.36}$	411^{+137}_{-168}	2
HIP 54849	A0V	11:13:45.55	-00:04:10.20	5.399	6.18	10000 ± 500	4.0 ± 0.25	$2.3^{+0.24}_{-0.21}$	72^{+197}_{-62}	2
HIP 55434	B9.5V	11:21:08.1934	+06:01:45.571	4.044	14.82	10618 ± 361	3.9 ± 0.14	$2.7^{+0.23}_{-0.19}$	304^{+32}_{-38}	1
HIP 56034	A2V	11:29:04.12	+39:20:13.11	5.354	15.33	10000 ± 500	4.5 ± 0.25	$2.2^{+0.15}_{-0.12}$	37^{+118}_{-29}	2
HIP 56633	B9.5V	11:36:40.91	-09:48:08.09	4.682	11.63	11524 ± 392	4.0 ± 0.14	$2.8^{+0.17}_{-0.12}$	145^{+105}_{-82}	1
HIP 57328	A4V	11:45:17.04	+08:15:29.21	4.845	26.73	8298 ± 282	4.3 ± 0.14	$1.9^{+0.14}_{-0.14}$	757^{+135}_{-265}	1
HIP 58590	A5V	12:00:52.39	+06:36:51.56	4.659	8.49	8000 ± 500	3.5 ± 0.25	$2.0^{+0.35}_{-0.35}$	618^{+300}_{-200}	2
HIP 59394	A1V	12:11:03.84	-23:36:08.72	5.470	17.00	9671 ± 329	4.3 ± 0.14	$2.1^{+0.10}_{-0.09}$	203^{+144}_{-128}	1
HIP 59449	B3V	12:11:39.12	-52:22:06.44	3.960	8.61	18000 ± 1000	4.5 ± 0.25	$5.4^{+0.61}_{-0.55}$	11^{+14}_{-5}	2
HIP 59819	A3V	12:16:00.19	+14:53:56.65	5.090	16.42	9528 ± 324	4.0 ± 0.14	$2.2^{+0.16}_{-0.14}$	394^{+95}_{-165}	1
HIP 60009	B2.5V	12:18:26.25	-64:00:11.05	4.050	9.12	20000 ± 1000	4.5 ± 0.25	$6.6^{+0.65}_{-0.66}$	9^{+9}_{-4}	2
HIP 60030	A5Vn	12:18:40.32	-00:47:13.87	5.908	8.73	7750 ± 1000	3.5 ± 0.25	$1.9^{+0.30}_{-0.39}$	778^{+807}_{-403}	2

TABLE 1 — *Continued*

star	SpT	RA	DEC	V	parallax (mas)	T_{eff} (K)	$\log g$ (cgs)	Mass (M_{\odot})	Age (Myr)	Ref
HIP 60595	A1V	12:25:11.76	-11:36:38.12	5.949	14.18	10396 ± 353	4.4 ± 0.14	$2.4^{+0.12}_{-0.10}$	161^{+111}_{-100}	1
HIP 60710	B3Vn	12:26:31.76	-51:27:02.29	4.805	7.28	20000 ± 1000	4.5 ± 0.25	$6.5^{+0.67}_{-0.63}$	9^{+9}_{-4}	2
HIP 60957	A3V	12:29:43.24	+20:53:45.99	5.680	11.90	9079 ± 309	3.9 ± 0.14	$2.1^{+0.15}_{-0.12}$	480^{+100}_{-192}	1
HIP 61558	A3V	12:36:47.35	-05:49:54.84	5.880	14.49	9600 ± 326	4.2 ± 0.14	$2.3^{+0.19}_{-0.16}$	436^{+57}_{-75}	1
HIP 61622	A2V	12:37:42.16	-48:32:28.69	3.860	24.85	10533 ± 358	4.0 ± 0.14	$2.3^{+0.25}_{-0.23}$	158^{+137}_{-102}	1
HIP 62541	A1V	12:48:54.21	+14:07:21.31	5.702	8.17	9250 ± 1000	4.0 ± 0.25	$2.0^{+0.36}_{-0.31}$	124^{+326}_{-110}	2
HIP 62576	A2V	12:49:17.45	+27:33:08.57	5.780	10.76	9955 ± 338	4.1 ± 0.14	$2.2^{+0.12}_{-0.11}$	188^{+132}_{-117}	1
HIP 63724	A0V	13:03:33.31	-49:31:38.15	4.830	14.79	10462 ± 356	4.1 ± 0.14	$2.4^{+0.12}_{-0.10}$	154^{+106}_{-96}	1
HIP 63945	B5V	13:06:16.70	-48:27:47.85	4.694	8.36	18000 ± 1000	4.5 ± 0.25	$5.4^{+0.61}_{-0.56}$	11^{+13}_{-6}	2
HIP 65198	A2V	13:21:41.64	+02:05:14.07	5.693	14.77	10291 ± 350	4.2 ± 0.14	$2.3^{+0.11}_{-0.10}$	174^{+111}_{-108}	1
HIP 65477	A5V	13:25:13.54	+54:59:16.65	4.010	39.91	8221 ± 280	4.2 ± 0.14	$1.8^{+0.16}_{-0.13}$	754^{+157}_{-222}	1
HIP 65728	A1Vn	13:28:27.09	+59:56:44.83	5.400	14.01	10388 ± 353	4.2 ± 0.14	$2.7^{+0.24}_{-0.19}$	331^{+39}_{-45}	1
HIP 66249	A2Van	13:34:41.74	-00:35:45.38	3.380	44.03	8542 ± 290	4.1 ± 0.14	$1.9^{+0.15}_{-0.12}$	631^{+113}_{-226}	1
HIP 66798	A2V	13:41:29.89	+64:49:20.68	5.850	14.66	9347 ± 318	4.2 ± 0.14	$2.1^{+0.11}_{-0.09}$	291^{+153}_{-170}	1
HIP 66821	B8.5Vn	13:41:44.77	-54:33:33.93	5.010	12.02	13141 ± 447	4.4 ± 0.14	$3.7^{+0.29}_{-0.24}$	138^{+12}_{-20}	1
HIP 67143	A0V	13:45:36.89	-26:06:57.63	5.805	11.49	10338 ± 351	4.3 ± 0.14	$2.3^{+0.11}_{-0.09}$	143^{+112}_{-93}	1
HIP 67194	A5V	13:46:13.55	+41:05:19.48	5.891	19.03	7953 ± 270	4.3 ± 0.14	$1.7^{+0.10}_{-0.09}$	504^{+325}_{-319}	1
HIP 67782	A8IV	13:53:10.28	+28:38:53.28	5.911	15.21	8051 ± 274	4.1 ± 0.14	$1.8^{+0.16}_{-0.12}$	846^{+121}_{-164}	1
HIP 68092	A8V	13:56:27.88	+01:03:02.09	5.906	11.08	7866 ± 267	3.9 ± 0.14	$1.6^{+0.07}_{-0.07}$	410^{+331}_{-274}	1
HIP 68520	A3V	14:01:38.79	+01:32:40.31	4.244	14.50	8413 ± 286	3.4 ± 0.14	$2.0^{+0.18}_{-0.12}$	722^{+118}_{-129}	1
HIP 70327	A0V	14:23:22.70	+08:26:47.84	5.120	15.17	9678 ± 329	4.0 ± 0.14	$2.2^{+0.12}_{-0.09}$	261^{+154}_{-316}	1
HIP 70384	A3V	14:24:00.88	+08:14:38.30	5.935	7.38	9000 ± 500	4.0 ± 0.25	$2.0^{+0.22}_{-0.18}$	99^{+316}_{-87}	2
HIP 70400	A3V	14:24:11.34	+05:49:12.47	5.103	20.51	8490 ± 289	4.2 ± 0.14	$1.8^{+0.08}_{-0.07}$	336^{+238}_{-215}	1
HIP 70915	B8Vn	14:30:08.63	-45:19:16.88	5.500	6.84	12000 ± 1000	4.5 ± 0.25	$2.8^{+0.42}_{-0.37}$	24^{+65}_{-17}	2
HIP 71865	B3V	14:41:57.59	-37:47:36.59	4.000	9.62	20000 ± 1000	4.5 ± 0.25	$6.6^{+0.66}_{-0.64}$	9^{+9}_{-4}	2
HIP 71974	B9.5V	14:43:13.55	-24:59:51.91	5.730	6.56	10000 ± 500	4.0 ± 0.25	$2.3^{+0.26}_{-0.22}$	65^{+210}_{-55}	2
HIP 72104	A0Vnn	14:44:59.20	-35:11:30.57	4.923	15.22	9618 ± 327	3.8 ± 0.14	$2.1^{+0.12}_{-0.09}$	239^{+143}_{-144}	1
HIP 72154	B9.5V	14:45:30.20	+00:43:02.19	5.673	6.61	10000 ± 500	4.0 ± 0.25	$2.3^{+0.24}_{-0.21}$	75^{+199}_{-65}	2
HIP 72250	A1V	14:46:28.99	-47:26:28.02	5.740	10.67	9784 ± 333	4.1 ± 0.14	$2.4^{+0.21}_{-0.18}$	411^{+49}_{-59}	1
HIP 72378	B9V	14:47:57.56	-26:38:46.16	5.768	7.29	9500 ± 1000	4.0 ± 0.25	$2.0^{+0.39}_{-0.31}$	103^{+291}_{-91}	2
HIP 72552	A4V	14:49:58.40	+28:36:57.00	5.800	10.16	9591 ± 326	3.9 ± 0.14	$2.2^{+0.14}_{-0.11}$	359^{+95}_{-168}	1
HIP 73049	A0V	14:55:44.71	-33:51:20.82	5.318	12.85	10108 ± 344	4.3 ± 0.14	$2.4^{+0.18}_{-0.14}$	337^{+53}_{-113}	1
HR 5605	B5V	15:05:07.18	-47:03:04.00	4.720	...	16000 ± 1000	4.5 ± 0.25	$4.5^{+0.53}_{-0.52}$	14^{+21}_{-8}	2
HIP 74117	B3V	15:08:50.62	-45:16:47.49	4.070	4.20	20000 ± 1000	4.5 ± 0.25	$6.6^{+0.67}_{-0.66}$	9^{+9}_{-4}	2
HIP 74689	A4V	15:15:49.08	+00:22:19.70	5.629	21.67	8255 ± 281	4.4 ± 0.14	$1.9^{+0.17}_{-0.14}$	780^{+102}_{-113}	1
HIP 75178	B9Vn	15:21:48.58	+32:56:01.30	5.375	12.45	12140 ± 413	4.3 ± 0.14	$3.3^{+0.26}_{-0.21}$	184^{+19}_{-28}	1
HIP 75304	B4V	15:23:09.35	-36:51:30.55	4.540	6.28	18000 ± 1000	4.5 ± 0.25	$5.4^{+0.58}_{-0.55}$	11^{+13}_{-6}	2
HIP 76267	A0V	15:34:41.27	+26:42:52.89	2.240	43.46	10342 ± 352	4.0 ± 0.14	$2.5^{+0.19}_{-0.16}$	313^{+53}_{-100}	1
HIP 76600	B2.5V	15:38:39.37	-29:46:39.89	3.644	8.89	20000 ± 1000	4.5 ± 0.25	$6.6^{+0.67}_{-0.66}$	9^{+9}_{-4}	2
HIP 76852	A1V	15:41:33.05	+19:40:13.44	4.509	17.16	9366 ± 318	4.1 ± 0.14	$2.0^{+0.09}_{-0.08}$	190^{+162}_{-123}	1
HIP 77233	A3V	15:46:11.25	+15:25:18.59	3.670	21.03	8928 ± 304	3.3 ± 0.14	$1.9^{+0.10}_{-0.08}$	332^{+201}_{-201}	1
HIP 77336	A3V	15:47:17.32	+14:06:55.26	5.712	13.04	8917 ± 303	4.0 ± 0.14	$2.9^{+0.23}_{-0.21}$	403^{+75}_{-21}	1
HIP 77516	A0V	15:49:37.21	-03:25:48.73	3.530	19.23	10000 ± 500	4.5 ± 0.25	$2.2^{+0.23}_{-0.19}$	37^{+113}_{-28}	2
HIP 77635	B1.5Vn	15:50:58.74	-25:45:04.66	4.638	6.59	24000 ± 1000	4.5 ± 0.25	$9.0^{+0.60}_{-0.67}$	7^{+4}_{-2}	2
HIP 77858	B5V	15:53:53.92	-24:31:59.37	5.376	7.76	16000 ± 1000	4.5 ± 0.25	$4.4^{+0.36}_{-0.49}$	13^{+21}_{-8}	2
HIP 78105	A3V	15:56:53.50	-33:57:58.01	5.080	23.60	9206 ± 313	4.1 ± 0.14	$2.0^{+0.12}_{-0.10}$	291^{+173}_{-171}	1
HIP 78106	B9V	15:56:54.12	-33:57:51.34	5.550	21.71	9725 ± 331	4.2 ± 0.14	$2.4^{+0.19}_{-0.15}$	412^{+50}_{-83}	1
HIP 78265	B1V	15:58:51.1132	-26:06:50.788	2.910	5.57
HIP 78554	A3V	16:02:17.69	+22:48:16.03	4.817	18.22	9226 ± 314	4.1 ± 0.14	$2.1^{+0.15}_{-0.13}$	464^{+88}_{-171}	1
HIP 78820	B1V	16:05:26.23	-19:48:19.63	2.620	8.07
HR 6025	A0Vn	16:06:19.6762	+67:48:36.480	5.439	12.85	9250 ± 1000	4.5 ± 0.25	$1.9^{+0.32}_{-0.31}$	48^{+210}_{-39}	2
HIP 78918	B2.5Vn	16:06:35.55	-36:48:08.26	4.205	7.87	20000 ± 1000	4.5 ± 0.25	$6.6^{+0.68}_{-0.63}$	9^{+9}_{-4}	2
HIP 78933	B1V	16:06:48.4269	-20:40:09.090	3.970	6.92
HIP 79005	B9V	16:07:36.42	-12:44:43.46	5.757	8.90	10000 ± 500	3.5 ± 0.25	$2.8^{+0.46}_{-0.42}$	281^{+84}_{-111}	2
HIP 79007	A7V	16:07:37.54	+09:53:30.27	5.639	10.10	7893 ± 268	3.9 ± 0.14	$1.6^{+0.08}_{-0.07}$	463^{+324}_{-301}	1
HIP 79199	B8V	16:09:52.59	-33:32:44.90	5.496	8.00	12000 ± 1000	4.5 ± 0.25	$2.8^{+0.40}_{-0.39}$	25^{+65}_{-17}	2
HIP 79387	A4V	16:12:07.32	-08:32:51.28	5.435	12.92	8418 ± 286	4.0 ± 0.14	$1.9^{+0.16}_{-0.12}$	694^{+108}_{-181}	1
HIP 79404	B2V	16:12:18.20	-27:55:34.95	4.567	6.81	22000 ± 1000	4.5 ± 0.25	$7.8^{+0.71}_{-0.68}$	8^{+6}_{-3}	2
HIP 79653	B8V	16:15:15.32	-47:22:19.27	5.124	8.46	14000 ± 1000	4.5 ± 0.25	$3.6^{+0.47}_{-0.44}$	17^{+35}_{-11}	2

TABLE 1 — *Continued*

star	SpT	RA	DEC	V	parallax (mas)	T_{eff} (K)	$\log g$ (cgs)	Mass (M_{\odot})	Age (Myr)	Ref
HIP 80460	A5V	16:25:24.17	+37:23:38.68	5.540	13.43	7810 ± 266	3.7 ± 0.14	$1.7^{+0.11}_{-0.08}$	783^{+229}_{-412}	1
HIP 80815	B3V	16:30:12.48	-25:06:54.80	4.790	7.89	22000 ± 1000	4.5 ± 0.25	$7.8^{+0.76}_{-0.71}$	8^{+6}_{-3}	2
HIP 80883	A0V	16:30:54.82	+01:59:02.12	3.900	18.84	9000 ± 500	4.0 ± 0.25	$2.0^{+0.22}_{-0.18}$	97^{+294}_{-86}	2
HIP 80991	A2V	16:32:25.68	+60:49:23.96	5.910	8.79	9000 ± 500	3.5 ± 0.25	$2.4^{+0.42}_{-0.39}$	405^{+134}_{-176}	2
HIP 81126	B9V	16:34:06.18	+42:26:13.34	4.196	10.36
HIP 81641	A1V	16:40:38.69	+04:13:11.23	5.772	11.11	10572 ± 359	4.1 ± 0.14	$2.6^{+0.21}_{-0.17}$	301^{+38}_{-66}	1
HIP 82350	A1V	16:49:34.66	+13:15:40.10	5.910	9.99	9630 ± 327	4.1 ± 0.14	$2.1^{+0.10}_{-0.08}$	207^{+145}_{-130}	1
HIP 82514	B1.5V	16:51:52.2311	-38:02:50.569	2.980	6.51	26000 ± 1000	4.5 ± 0.25	$9.6^{+0.58}_{-0.43}$	5^{+3}_{-1}	2
HIP 82673	B8V	16:54:00.47	+10:09:55.30	4.380	13.30	12000 ± 1000	3.8 ± 0.25	$3.1^{+0.58}_{-0.45}$	118^{+82}_{-98}	2
HIP 83635	B1V	17:05:32.26	-00:53:31.45	5.610	2.92
HIP 84606	A2V	17:17:40.25	+37:17:29.40	4.650	18.59	9702 ± 330	4.0 ± 0.14	$2.1^{+0.10}_{-0.09}$	155^{+137}_{-100}	1
HIP 85290	A1Vn	17:25:41.35	+60:02:54.23	5.645	10.32	10989 ± 374	4.0 ± 0.14	$2.5^{+0.12}_{-0.11}$	110^{+88}_{-70}	1
HIP 85379	A4V	17:26:44.24	+48:15:36.23	5.830	8.68	8000 ± 500	3.5 ± 0.25	$2.0^{+0.42}_{-0.32}$	621^{+266}_{-320}	2
HIP 85385	B5V	17:26:49.13	+20:04:51.52	5.510	5.59
HIP 85537	A8Vp	17:28:49.65	+00:19:50.25	5.424	16.77	7624 ± 259	3.8 ± 0.14	$1.8^{+0.16}_{-0.14}$	1064^{+148}_{-159}	1
HIP 85727	B8Vn	17:31:05.91	-60:41:01.85	3.620	16.48	12740 ± 433	4.0 ± 0.14	$3.2^{+0.15}_{-0.13}$	92^{+48}_{-54}	1
HIP 85922	A5V	17:33:29.85	-05:44:41.29	5.619	20.79	8000 ± 500	4.0 ± 0.25	$1.7^{+0.19}_{-0.16}$	117^{+539}_{-105}	2
HIP 86019	B8Vn	17:34:46.35	-11:14:31.19	5.537	8.11	12000 ± 1000	4.5 ± 0.25	$2.8^{+0.42}_{-0.37}$	25^{+62}_{-17}	2
HIP 86782	A2V	17:43:59.18	+53:48:06.17	5.760	6.12	10000 ± 500	4.0 ± 0.25	$2.3^{+0.25}_{-0.22}$	58^{+207}_{-49}	2
HIP 87108	A0Vn	17:47:53.56	+02:42:26.20	3.750	31.73	10075 ± 343	4.2 ± 0.14	$2.3^{+0.15}_{-0.12}$	258^{+101}_{-138}	1
HIP 88116	A0	17:59:47.56	-23:48:58.09	4.731	7.85	10000 ± 500	4.0 ± 0.25	$2.3^{+0.25}_{-0.20}$	76^{+200}_{-66}	2
HIP 88290	A2Vn	18:01:45.20	+01:18:18.28	4.439	11.15	10010 ± 340	3.8 ± 0.14	$2.3^{+0.12}_{-0.11}$	243^{+112}_{-140}	1
HIP 88818	A3V	18:07:49.45	+26:06:04.13	5.870	20.16	9162 ± 312	4.3 ± 0.14	$2.7^{+0.24}_{-0.23}$	442^{+86}_{-70}	1
HIP 88817	A3V	18:07:49.50	+26:05:50.40	5.900	25.92	9162 ± 312	4.3 ± 0.14	$2.1^{+0.15}_{-0.12}$	481^{+83}_{-173}	1
HIP 89156	A3V	18:11:45.12	+33:26:49.41	5.970	4.21	9000 ± 500	3.5 ± 0.25	$2.4^{+0.39}_{-0.39}$	410^{+157}_{-108}	2
HIP 89935	A7V	18:21:01.02	+28:52:11.83	5.129	12.40	7594 ± 258	3.4 ± 0.14	$2.3^{+0.10}_{-0.13}$	727^{+108}_{-70}	1
HIP 90052	A2V	18:22:35.32	+12:01:46.85	5.980	7.42	9000 ± 500	3.5 ± 0.25	$2.4^{+0.40}_{-0.40}$	404^{+175}_{-175}	2
HIP 90762	A2V	18:31:04.45	+16:55:42.80	5.760	7.49	8750 ± 1000	3.5 ± 0.25	$2.2^{+0.54}_{-0.46}$	482^{+375}_{-247}	2
HIP 90887	A3Vn	18:32:21.33	-39:42:14.40	5.162	14.23	9403 ± 320	4.1 ± 0.14	$2.1^{+0.14}_{-0.12}$	335^{+143}_{-187}	1
HIP 91118	A0Vn	18:35:12.60	+18:12:12.28	5.790	5.04	9500 ± 1000	4.0 ± 0.25	$2.1^{+0.32}_{-0.32}$	111^{+276}_{-98}	2
HIP 91875	A2Vn	18:43:46.94	-38:19:24.39	5.120	15.89	9287 ± 316	4.0 ± 0.14	$2.1^{+0.10}_{-0.10}$	339^{+188}_{-189}	1
HIP 92027	A1V	18:45:28.36	+05:30:00.44	5.830	5.30	9000 ± 500	3.5 ± 0.25	$2.4^{+0.43}_{-0.37}$	406^{+140}_{-167}	2
HIP 92312	A1V	18:48:53.39	+19:19:43.40	5.894	11.41	9923 ± 337	4.2 ± 0.14	$2.2^{+0.10}_{-0.09}$	164^{+128}_{-105}	1
HIP 92728	B2.5V	18:53:43.56	+36:58:18.19	5.569	3.29	20000 ± 1000	4.5 ± 0.25	$6.6^{+0.68}_{-0.61}$	9^{+9}_{-4}	2
HIP 92855	B2V	18:55:15.93	-26:17:48.21	2.058	14.32	19192 ± 653	4.3 ± 0.14	$6.3^{+0.38}_{-0.28}$	29^{+6}_{-12}	1
HIP 92946	A5V	18:56:13.18	+04:12:12.91	4.620	21.09	7968 ± 271	4.1 ± 0.14	$1.6^{+0.19}_{-0.23}$	658^{+683}_{-409}	1
HIP 93225	B4V	18:59:23.80	-12:50:25.86	5.516	6.84	15000 ± 1000	3.8 ± 0.25	$4.4^{+0.71}_{-0.55}$	54^{+34}_{-42}	2
HIP 93393	B5V	19:01:17.36	+26:17:29.08	5.683	5.02	18000 ± 1000	4.5 ± 0.25	$5.4^{+0.60}_{-0.55}$	11^{+13}_{-5}	2
HIP 93580	A4V	19:03:32.25	+01:49:07.57	5.826	18.22	8224 ± 280	4.3 ± 0.14	$1.8^{+0.12}_{-0.10}$	590^{+236}_{-315}	1
HIP 93713	A0Vn	19:04:55.17	+53:23:47.96	5.380	9.00	9000 ± 1000	4.0 ± 0.25	$1.9^{+0.36}_{-0.31}$	129^{+363}_{-115}	2
HIP 93747	A0Vn	19:05:24.61	+13:51:48.52	2.990	39.28	11409 ± 388	4.2 ± 0.14	$3.3^{+0.29}_{-0.25}$	231^{+23}_{-26}	1
HIP 93805	B9Vn	19:06:14.94	-04:52:57.20	3.430	26.37	11962 ± 407	4.2 ± 0.14	$3.5^{+0.33}_{-0.27}$	194^{+20}_{-22}	1
HIP 94620	A4V	19:15:17.36	+21:13:55.62	5.654	10.89	9190 ± 312	4.0 ± 0.14	$2.0^{+0.09}_{-0.07}$	202^{+169}_{-130}	1
HIP 94720	B9.5V	19:16:26.79	+14:32:40.62	5.630	7.96	10000 ± 500	4.0 ± 0.25	$2.3^{+0.25}_{-0.20}$	69^{+194}_{-58}	2
HIP 95241	B9V	19:22:38.30	-44:27:32.25	4.010	10.40	12000 ± 1000	4.0 ± 0.25	$2.9^{+0.50}_{-0.41}$	53^{+108}_{-43}	2
HIP 95560	A0V	19:26:13.25	+20:05:51.84	5.594	13.72	9250 ± 1000	4.5 ± 0.25	$1.9^{+0.32}_{-0.29}$	45^{+197}_{-37}	2
HIP 95619	B8.5V	19:26:56.48	-29:44:35.62	5.650	14.30	11997 ± 408	4.3 ± 0.14	$2.9^{+0.15}_{-0.12}$	107^{+60}_{-63}	1
HIP 95853	A5V	19:29:42.36	+51:43:47.21	3.769	26.88	8216 ± 279	3.9 ± 0.14	$1.8^{+0.14}_{-0.11}$	693^{+186}_{-300}	1
HIP 96288	A2V	19:34:41.26	+42:24:45.04	5.348	5.66	9000 ± 500	3.5 ± 0.25	$2.4^{+0.43}_{-0.39}$	405^{+137}_{-166}	2
HIP 97376	B8Vn	19:47:27.78	+38:24:27.41	5.826	6.90	11500 ± 2000	4.5 ± 0.25	$2.2^{+0.73}_{-0.70}$	34^{+157}_{-26}	2
HIP 97496	A3V	19:48:58.66	+19:08:31.35	5.000	12.79	8422 ± 286	3.9 ± 0.14	$1.8^{+0.09}_{-0.07}$	435^{+227}_{-265}	1
HIP 97870	B5V	19:53:17.38	+57:31:24.53	5.132	5.15	16000 ± 1000	4.0 ± 0.25	$4.7^{+0.64}_{-0.53}$	26^{+32}_{-19}	2
HIP 97966	B7Vn	19:54:37.65	-08:13:38.24	5.710	6.76	14000 ± 1000	4.2 ± 0.25	$3.6^{+0.47}_{-0.46}$	24^{+45}_{-16}	2
HIP 98055	A4Vn	19:55:37.79	+52:26:20.21	4.920	11.59	9000 ± 500	4.5 ± 0.25	$1.9^{+0.18}_{-0.17}$	47^{+186}_{-38}	2
HIP 98325	B9Vn	19:58:37.98	+30:59:01.19	5.506	7.01	12000 ± 1000	4.5 ± 0.25	$2.8^{+0.41}_{-0.37}$	25^{+65}_{-17}	2
HIP 99080	B3V	20:06:53.41	+23:36:51.93	5.064	6.47	20000 ± 1000	4.5 ± 0.25	$6.6^{+0.68}_{-0.64}$	9^{+9}_{-4}	2
HIP 99742	A1Va	20:14:16.62	+15:11:51.39	4.947	21.75	9645 ± 328	4.3 ± 0.14	$2.3^{+0.17}_{-0.14}$	412^{+59}_{-116}	1
HIP 100069	B0V	20:18:06.99	+40:43:55.50	5.840	1.68
HIP 100221	B9V	20:19:36.72	+62:15:26.90	5.712	8.63	10000 ± 500	4.0 ± 0.25	$2.3^{+0.25}_{-0.21}$	70^{+205}_{-60}	2

TABLE 1 — *Continued*

star	SpT	RA	DEC	V	parallax (mas)	T_{eff} (K)	$\log g$ (cgs)	Mass (M_{\odot})	Age (Myr)	Ref
HIP 100907	A3V	20:27:34.26	+38:26:25.19	5.620	12.28	9042 ± 307	4.0 ± 0.14	2.1 ^{+0.16} _{-0.13}	514 ⁺⁹⁹ ₋₁₆₆	1
HIP 101123	A1V	20:29:53.91	-18:34:59.48	5.906	15.07	10492 ± 357	4.2 ± 0.14	2.4 ^{+0.11} _{-0.09}	143 ⁺¹⁰⁹ ₋₉₁	1
HIP 101589	A3V	20:35:18.54	+14:40:27.17	4.664	14.82	8639 ± 294	3.8 ± 0.14	2.0 ^{+0.15} _{-0.12}	624 ⁺⁹⁸ ₋₁₇₆	1
HIP 101716	B8V	20:37:04.67	+26:27:43.01	5.589	10.27	12949 ± 440	4.2 ± 0.14	3.3 ^{+0.17} _{-0.14}	91 ⁺⁴⁴ ₋₅₃	1
HIP 101909	B3V	20:39:04.97	+15:50:17.52	5.980	2.42
HIP 102487	A1V	20:46:09.99	-21:30:50.52	5.913	12.37	9702 ± 330	4.1 ± 0.14	2.1 ^{+0.11} _{-0.09}	180 ⁺¹⁴³ ₋₁₁₆	1
HIP 103298	A5V	20:55:38.57	+12:34:06.81	5.540	16.53	9093 ± 309	4.1 ± 0.14	2.0 ^{+0.13} _{-0.11}	400 ⁺¹⁵⁰ ₋₂₁₅	1
HIP 104105	B8Vn	21:05:29.27	+78:07:35.02	5.915	8.10	9750 ± 1000	4.0 ± 0.25	2.1 ^{+0.39} _{-0.32}	92 ⁺²⁵⁵ ₋₈₀	2
HIP 104139	A1V	21:05:56.83	-17:13:58.30	4.070	20.11	10001 ± 340	4.2 ± 0.14	2.2 ^{+0.11} _{-0.09}	187 ⁺¹³⁰ ₋₁₁₆	1
HIP 104365	A0V	21:08:33.63	-21:11:37.22	5.280	18.14	10878 ± 370	4.3 ± 0.14	2.8 ^{+0.21} _{-0.17}	272 ⁺³³ ₋₅₃	1
HIP 105140	A1V	21:17:56.28	-32:10:21.15	4.721	17.90	9126 ± 310	4.4 ± 0.14	2.3 ^{+0.21} _{-0.18}	538 ⁺⁶⁹ ₋₇₀	1
HIP 105282	B6V	21:19:28.75	+49:30:37.06	5.740	5.98	16000 ± 1000	4.5 ± 0.25	4.5 ^{+0.53} _{-0.51}	13 ⁺²¹ ₋₇	2
HIP 105891	B6V	21:26:44.97	+52:53:54.73	5.989	7.28	10500 ± 2000	4.0 ± 0.25	2.1 ^{+0.71} _{-0.58}	102 ⁺⁴⁰⁴ ₋₈₉	2
HIP 105942	B3V	21:27:21.37	+37:07:00.47	5.289	2.50	20000 ± 1000	4.5 ± 0.25	6.6 ^{+0.69} _{-0.64}	9 ⁺⁹ ₋₄	2
HIP 105966	A1V	21:27:40.06	+27:36:30.94	5.389	17.14	9622 ± 327	4.3 ± 0.14	2.1 ^{+0.12} _{-0.10}	263 ⁺¹³⁸ ₋₁₅₆	1
HIP 105972	B7V	21:27:46.14	+66:48:32.74	5.407	4.05	14000 ± 1000	4.0 ± 0.25	3.8 ^{+0.53} _{-0.48}	38 ⁺⁵⁴ ₋₂₉	2
HIP 106711	A3Vn	21:36:56.98	+40:24:48.67	5.052	15.19	7859 ± 267	3.9 ± 0.14	1.7 ^{+0.11} _{-0.08}	767 ⁺²²⁶ ₋₃₈₇	1
HIP 106786	A7V	21:37:45.11	-07:51:15.13	4.690	18.26	8140 ± 277	4.0 ± 0.14	1.7 ^{+0.10} _{-0.07}	567 ⁺²³⁹ ₋₃₂₆	1
HIP 107517	A1V	21:46:32.10	-11:21:57.44	5.570	11.58	10674 ± 363	4.2 ± 0.14	2.5 ^{+0.14} _{-0.11}	191 ⁺⁸⁹ ₋₁₀₈	1
HIP 107608	A2V	21:47:44.15	-30:53:53.90	5.016	10.16	9716 ± 330	4.0 ± 0.14	2.2 ^{+0.15} _{-0.12}	342 ⁺⁹³ ₋₁₆₁	1
HIP 108294	A2Vn	21:56:22.77	-37:15:13.16	5.457	9.71	9000 ± 500	4.0 ± 0.25	2.0 ^{+0.22} _{-0.18}	93 ⁺³¹⁸ ₋₈₁	2
HIP 108339	A2Vnn	21:56:56.37	+12:04:35.37	5.544	8.14	9250 ± 1000	4.0 ± 0.25	2.0 ^{+0.35} _{-0.31}	121 ⁺³¹⁶ ₋₁₀₉	2
HIP 109056	B9Vn	22:05:34.67	+28:57:50.32	5.700	9.40	9800 ± 1200	4.4 ± 0.25	2.0 ^{+0.41} _{-0.36}	51 ⁺²⁰⁰ ₋₄₂	2
HIP 109139	B8V	22:06:26.23	-13:52:10.86	4.270	18.62	12641 ± 430	4.3 ± 0.14	3.2 ^{+0.20} _{-0.16}	124 ⁺³⁷ ₋₆₂	1
HIP 109521	A5V	22:11:09.89	+50:49:24.26	5.386	17.81	8420 ± 286	4.2 ± 0.14	2.0 ^{+0.19} _{-0.16}	728 ⁺¹⁰⁷ ₋₁₀₆	1
HIP 109831	A2Vnn	22:14:44.37	+42:57:14.07	5.720	12.14	10932 ± 372	4.2 ± 0.14	2.5 ^{+0.13} _{-0.12}	123 ⁺⁹² ₋₇₉	1
HIP 110838	B9Vn	22:27:19.97	-64:57:58.88	4.495	13.00	11271 ± 383	4.1 ± 0.14	3.0 ^{+0.24} _{-0.20}	243 ⁺²⁴ ₋₃₃	1
HIP 110935	A4V	22:28:37.67	-67:29:20.62	5.570	23.19	8026 ± 273	4.3 ± 0.14	1.7 ^{+0.08} _{-0.07}	447 ⁺³⁰¹ ₋₂₉₁	1
HIP 111056	A3V	22:29:52.98	+78:49:27.43	5.460	13.31	8750 ± 1000	4.2 ± 0.25	1.8 ^{+0.33} _{-0.30}	85 ⁺³⁴⁷ ₋₇₄	2
HIP 111068	B9.5V	22:30:01.81	+32:34:21.50	5.650	9.05	10000 ± 500	3.5 ± 0.25	2.8 ^{+0.47} _{-0.42}	280 ⁺⁸⁵ ₋₁₁₂	2
HIP 111169	A1V	22:31:17.50	+50:16:56.97	3.770	31.79	10071 ± 342	4.3 ± 0.14	2.3 ^{+0.12} _{-0.10}	202 ⁺¹²³ ₋₁₂₃	1
HIP 112029	B8V	22:41:27.73	+10:49:52.64	3.410	...	11913 ± 405	3.8 ± 0.14	2.9 ^{+0.17} _{-0.14}	135 ⁺⁵⁷ ₋₇₆	1
HIP 113788	A1V	23:02:36.38	+42:45:28.06	...	7.74	9000 ± 500	4.0 ± 0.25	2.0 ^{+0.22} _{-0.18}	100 ⁺³⁰⁹ ₋₈₈	2
HIP 114520	A5Vn	23:11:44.19	+08:43:12.40	5.157	13.46	8220 ± 279	3.8 ± 0.14	1.7 ^{+0.10} _{-0.08}	437 ⁺²⁷⁷ ₋₂₇₀	1
HIP 114822	A2V	23:15:34.26	-03:29:46.96	5.550	14.04	9678 ± 329	4.1 ± 0.14	2.2 ^{+0.12} _{-0.10}	255 ⁺¹³⁶ ₋₁₅₃	1
HIP 115115	A0V	23:18:57.68	-09:36:38.70	5.001	12.47	10671 ± 363	4.2 ± 0.14	2.6 ^{+0.20} _{-0.16}	284 ⁺³⁸ ₋₇₉	1
HIP 116247	A0V	23:33:16.62	-20:54:52.21	4.709	11.11	10267 ± 349	3.9 ± 0.14	2.5 ^{+0.20} _{-0.16}	334 ⁺⁴⁶ ₋₇₈	1
HIP 116582	B8V	23:37:32.04	+44:25:44.37	5.817	4.04	12000 ± 1000	4.0 ± 0.25	2.9 ^{+0.46} _{-0.43}	54 ⁺¹⁰⁴ ₋₄₄	2
HIP 116611	A0Vn	23:37:56.80	+18:24:02.40	5.482	14.01	11060 ± 376	4.1 ± 0.14	2.7 ^{+0.19} _{-0.15}	228 ⁺⁴⁶ ₋₉₂	1
HIP 116631	B8V	23:38:08.20	+43:16:05.06	4.290	6.53	12000 ± 1000	3.8 ± 0.25	3.1 ^{+0.55} _{-0.48}	116 ⁺⁸² ₋₉₆	2
HIP 116805	A0V	23:40:24.51	+44:20:02.16	4.140	19.37	11903 ± 405	4.3 ± 0.14	2.9 ^{+0.17} _{-0.14}	145 ⁺⁵¹ ₋₇₄	1
HIP 116971	B9V	23:42:43.34	-14:32:41.65	4.483	21.96	11108 ± 378	4.3 ± 0.14	2.6 ^{+0.15} _{-0.14}	109 ⁺⁹⁰ ₋₇₀	1
HIP 117089	B9V	23:44:12.08	-18:16:36.97	5.235	8.61	12000 ± 1000	4.5 ± 0.25	2.8 ^{+0.40} _{-0.37}	24 ⁺⁶³ ₋₁₇	2
HIP 117371	A1Vn	23:47:54.77	+67:48:24.51	5.048	10.76	10308 ± 350	3.9 ± 0.14	2.5 ^{+0.19} _{-0.17}	323 ⁺⁵³ ₋₉₂	1
HIP 117452	A0Vn	23:48:55.55	-28:07:48.97	4.570	23.73	11417 ± 388	4.3 ± 0.14	3.0 ^{+0.26} _{-0.22}	233 ⁺³² ₋₃₇	1
HIP 118121	A1V	23:57:35.08	-64:17:53.63	5.002	21.08	9979 ± 339	4.3 ± 0.14	2.3 ^{+0.16} _{-0.13}	335 ⁺⁷⁰ ₋₁₃₄	1
HIP 118243	B1V	23:59:00.54	+55:45:17.74	4.997	0.72

NOTE. — The spectral types, coordinates, V-band magnitudes, and parallax measurements are taken from the Simbad database; the spectral type given is that of the brightest star if part of a known multiple system. The "Ref" column denotes the reference for the stellar effective temperature, surface gravity, mass, and age. The references are: [1]: (David & Hillenbrand 2015); [2]: This study.

TABLE 2
SPECTROSCOPIC OBSERVATION LOG

star	MJD (JD-2450000)	instrument	exptime (sec)	snr
HIP 813	6618.58	TS23	557	1810
HIP 1191	6552.60	CHIRON	1200	320
HIP 1366	6585.73	TS23	274	1790
HIP 1647	6510.74	CHIRON	1105	630
HIP 2381	6874.71	CHIRON	505	580
HIP 2505	6586.71	TS23	235	1700
HIP 2505	6962.71	TS23	804	1960
HIP 2505	6945.71	IGRINS	224	210
HIP 2548	7240.93	IGRINS	360	100
HIP 2548	6516.84	HRS	412	1070
HIP 3300	6299.55	TS23	689	1010
HIP 3478	6963.63	TS23	1200	1020
HIP 3478	7288.82	IGRINS	540	30
HIP 3478	6669.53	TS23	743	1870
HIP 3478	6945.72	IGRINS	224	150
HIP 5131	6587.70	TS23	655	1780
HIP 5131	7083.57	IGRINS	930	70
HIP 5131	6847.89	IGRINS	1600	110
HIP 5132	6587.77	TS23	535	1550
HIP 5132	6847.89	IGRINS	480	110
HIP 5310	6945.75	IGRINS	224	200
HIP 5361	6523.84	HRS	1000	810
HIP 5518	7238.94	IGRINS	540	80
HIP 5518	6945.77	IGRINS	224	160
HIP 5626	6945.88	IGRINS	224	160
HIP 7345	6888.76	CHIRON	1080	480
HIP 7345	6887.76	CHIRON	706	540
HIP 8016	6522.96	HRS	328	580
HIP 8704	6506.90	HRS	365	420
HIP 8704	7084.57	IGRINS	960	30
HIP 8704	7237.93	IGRINS	720	90
HR 545	6668.56	TS23	597	1920
HR 545	6586.75	TS23	265	1710
HR 545	6945.81	IGRINS	224	230
HIP 9312	6586.78	TS23	419	1750
HIP 9564	6945.78	IGRINS	224	140
HR 604	6585.86	TS23	349	1650
HIP 10320	6532.80	CHIRON	1020	550
HIP 10670	6618.68	TS23	141	1810
HIP 10732	6945.82	IGRINS	224	180
HIP 10732	7083.56	IGRINS	240	110
HIP 11345	6894.90	CHIRON	540	520
HIP 12332	6677.54	TS23	1107	1530
HIP 12332	6947.79	IGRINS	224	170
HIP 12706	6584.86	TS23	362	990
HIP 12706	6946.84	IGRINS	224	150
HIP 12719	6583.87	TS23	264	1720
HIP 12803	6676.53	TS23	452	1410
HIP 12803	6947.80	IGRINS	224	140
HIP 12803	7240.95	IGRINS	780	120
HIP 13165	6518.91	HRS	275	850
HIP 13202	6910.83	CHIRON	580	570
HIP 13209	6618.66	TS23	143	1880
HIP 13327	6670.54	TS23	1200	1800
HIP 13717	6917.83	CHIRON	644	550
HIP 13717	6970.75	CHIRON	703	550
HIP 13879	6945.79	IGRINS	224	260
HIP 13879	6681.68	TS23	930	230
HIP 13879	6618.70	TS23	265	1490
HIP 14043	6523.92	HRS	400	620
HIP 14293	6919.89	CHIRON	800	240
HIP 14764	6679.53	TS23	532	1370
HIP 14764	6946.80	IGRINS	360	150
HIP 14862	6945.86	IGRINS	224	180
HIP 14862	7084.60	IGRINS	1200	120
HIP 15110	6946.83	IGRINS	224	120
HIP 15338	6523.90	HRS	570	690
HIP 15404	6517.92	HRS	205	620
HIP 15444	6582.94	TS23	340	1790
HIP 16210	6676.58	TS23	406	1440
HIP 16210	6945.84	IGRINS	224	160
HIP 16244	6583.84	TS23	311	1750
HIP 16244	6945.83	IGRINS	224	230
HIP 16285	6933.84	CHIRON	767	570
HIP 16322	6944.72	CHIRON	680	410

TABLE 2 — *Continued*

star	MJD (JD-2450000)	instrument	exptime (sec)	snr
HIP 16322	6946.82	IGRINS	224	170
HIP 16340	6678.54	TS23	570	1410
HIP 16599	6945.85	IGRINS	224	170
HIP 16611	6946.85	IGRINS	224	210
HIP 16611	6522.88	CHIRON	255	580
HIP 17457	6531.82	CHIRON	1005	520
HIP 17527	6947.82	IGRINS	224	120
HIP 17527	6517.93	HRS	429	670
HIP 17527	6963.91	TS23	818	470
HIP 17563	6538.82	CHIRON	1088	400
HIP 18141	6678.59	TS23	605	1430
HIP 18396	6516.94	HRS	259	510
HIP 18788	6535.81	CHIRON	1039	180
HIP 18805	6585.78	TS23	631	1760
HIP 19799	6668.63	TS23	1200	1900
HIP 19949	6945.90	IGRINS	224	220
HIP 19949	7084.62	IGRINS	960	30
HIP 19968	6676.62	TS23	524	1390
HIP 20264	6718.53	CHIRON	860	410
HIP 20380	6945.89	IGRINS	224	180
HIP 20380	7084.67	IGRINS	1200	30
HIP 20430	6520.95	HRS	360	710
HIP 20507	6719.50	CHIRON	715	470
HIP 20579	6517.96	HRS	490	830
HIP 20789	6946.86	IGRINS	224	150
HIP 20789	6586.83	TS23	524	1610
HIP 21589	6962.94	TS23	220	1020
HIP 21589	7065.63	CHIRON	754	290
HIP 21589	6948.96	IGRINS	112	140
HIP 21683	6948.98	IGRINS	230	110
HIP 21683	6962.97	TS23	335	1040
HIP 21819	6679.64	TS23	466	1480
HIP 21928	6677.63	TS23	1124	1470
HIP 22028	6947.90	IGRINS	240	140
HIP 22509	6667.62	TS23	1200	1100
HIP 22509	7126.51	CHIRON	2612	440
HIP 22833	6679.60	TS23	521	1520
HIP 22833	6946.87	IGRINS	224	140
HIP 22840	6678.64	TS23	528	1380
HIP 22913	6585.74	CHIRON	1200	230
HIP 22958	6551.79	CHIRON	1200	340
HIP 22958	6943.77	CHIRON	650	320
HIP 23362	6548.87	CHIRON	725	520
HIP 23362	6946.93	IGRINS	240	180
HIP 23916	6555.82	CHIRON	1200	40
HIP 23916	6946.95	IGRINS	280	140
HIP 24244	6949.84	CHIRON	370	560
HIP 24244	6554.91	CHIRON	488	330
HIP 2427	6529.88	CHIRON	277	560
HIP 24505	7036.69	CHIRON	2045	480
HIP 24902	6946.88	IGRINS	224	180
HIP 24902	ADS 3962 AB			
HIP 25143	6946.92	IGRINS	280	170
HIP 25143	7084.65	IGRINS	960	80
HIP 25143	6946.89	IGRINS	224	180
HIP 25280	6950.75	CHIRON	597	540
HIP 25280	6947.91	IGRINS	240	130
HIP 25555	6670.63	TS23	600	1950
HIP 25608	6718.62	CHIRON	1030	360
HIP 25695	6669.65	TS23	1200	1860
HIP 25790	6946.90	IGRINS	224	160
HIP 25813	7083.58	IGRINS	1020	200
HIP 25813	6544.88	CHIRON	384	260
HIP 26063	6582.80	CHIRON	1139	250
HIP 26093	6946.91	IGRINS	280	150
HIP 26093	6676.66	TS23	525	1380
HIP 26093	7084.72	IGRINS	1800	90
HIP 26126	6946.96	IGRINS	240	170
HIP 26126	6721.50	CHIRON	507	450
HIP 26126	6948.81	CHIRON	550	360
HIP 26563	6677.68	TS23	502	1550
HIP 27100	6692.59	CHIRON	294	680
HIP 27100	6727.54	CHIRON	177	560
HIP 27321	6696.62	CHIRON	178	640
HIP 27713	6946.97	IGRINS	240	150
HIP 28691	6298.78	TS23	646	1300
HIP 28756	6571.74	CHIRON	1200	320

TABLE 2 — *Continued*

star	MJD (JD-2450000)	instrument	exptime (sec)	snr
HIP 28910	6693.61	CHIRON	343	560
HIP 29150	6697.63	CHIRON	950	380
HIP 29151	6946.99	IGRINS	264	170
HIP 29151	6953.82	CHIRON	617	540
HIP 29735	6559.80	CHIRON	803	380
HIP 29735	6946.98	IGRINS	240	170
HIP 29997	6679.70	TS23	415	1460
HIP 30069	6573.75	CHIRON	1200	250
HIP 30073	6581.82	CHIRON	1011	280
HIP 30666	6947.00	IGRINS	280	160
HIP 30788	6574.75	CHIRON	488	340
HIP 31278	7084.69	IGRINS	960	90
HIP 31278	6668.71	TS23	797	1920
HIP 31278	6947.01	IGRINS	280	170
HIP 31362	6598.72	CHIRON	1200	250
HIP 31434	6676.71	TS23	611	1480
HIP 32474	6592.74	CHIRON	1200	340
HIP 32607	7037.75	CHIRON	56	210
HIP 32607	7039.62	CHIRON	49	210
HIP 32607	6724.56	CHIRON	67	560
HIP 33372	6948.00	IGRINS	320	110
HIP 33372	6678.72	TS23	720	1380
HIP 34769	6677.75	TS23	279	1520
HIP 35180	6696.76	CHIRON	925	290
HIP 35341	6680.75	TS23	833	1070
HIP 36393	6676.76	TS23	616	1550
HIP 36393	6670.76	TS23	494	1400
HIP 36760	7084.74	IGRINS	720	150
HIP 36760	7037.76	CHIRON	4284	370
HIP 36760	7039.68	CHIRON	3127	480
HIP 36760	6668.79	TS23	836	700
HIP 36812	6947.99	IGRINS	280	110
HIP 36917	6583.81	CHIRON	571	420
HIP 36917	6971.83	CHIRON	435	690
HIP 37297	6698.74	CHIRON	370	480
HIP 37297	6574.82	CHIRON	686	340
HIP 37297	6729.53	CHIRON	231	460
HIP 37322	6975.79	CHIRON	817	540
HIP 37450	6600.74	CHIRON	1171	450
HIP 38538	6669.78	TS23	474	1990
HIP 38593	7039.70	CHIRON	331	170
HIP 38593	6599.82	CHIRON	1200	410
HIP 38593	6592.87	CHIRON	1200	300
HIP 38846	6601.76	CHIRON	1098	400
HIP 39095	6765.53	CHIRON	430	450
HIP 39095	6757.56	CHIRON	238	490
HIP 39095	6711.62	CHIRON	288	500
HIP 39236	6679.73	TS23	730	1420
HIP 39567	6668.80	TS23	613	1940
HIP 39847	7084.68	IGRINS	480	160
HIP 39847	6676.80	TS23	402	1500
HIP 39906	6580.86	CHIRON	457	270
HIP 40429	6691.72	CHIRON	710	560
HIP 40706	6327.64	CHIRON	277	630
HIP 40881	6947.97	IGRINS	240	100
HIP 41039	7039.73	CHIRON	1728	530
HIP 41039	6330.77	CHIRON	404	400
HIP 41307	6667.82	TS23	700	1220
HIP 42090	7124.62	IGRINS	630	120
HIP 42129	6603.80	CHIRON	1001	370
HIP 42313	6681.81	TS23	489	1020
HIP 42334	6712.64	CHIRON	381	480
HIP 43142	6670.79	TS23	647	1980
HIP 44127	6677.88	TS23	239	1600
HIP 44307	6947.98	IGRINS	280	80
HIP 45336	6328.70	CHIRON	171	290
HIP 45336	7122.66	IGRINS	270	130
HIP 45336	7084.75	IGRINS	240	140
HIP 45344	6612.79	CHIRON	1001	320
HIP 45688	6299.93	TS23	600	880
HIP 46225	6679.84	TS23	933	1300
HIP 46283	6732.56	CHIRON	357	490
HIP 46283	6619.80	CHIRON	872	430
HIP 46283	6712.70	CHIRON	352	450
HIP 46897	7084.78	IGRINS	1200	20
HIP 46897	7139.59	IGRINS	720	120

TABLE 2 — *Continued*

star	MJD (JD-2450000)	instrument	exptime (sec)	snr
HIP 47006	6677.03	TS23	373	1590
HIP 47175	6424.56	CHIRON	264	660
HIP 50303	6677.78	TS23	1200	1350
HIP 50860	6678.81	TS23	1151	1470
HIP 51362	7043.79	CHIRON	1298	340
HIP 51362	6625.81	CHIRON	947	200
HIP 51362	6673.75	CHIRON	606	510
HIP 51362	7084.76	IGRINS	720	100
HIP 51685	6677.90	TS23	1046	1460
HIP 52422	6676.87	TS23	522	1540
HIP 52457	6676.83	TS23	647	1500
HIP 52638	6669.83	TS23	711	1900
HIP 52678	6748.56	CHIRON	375	500
HIP 52678	6690.70	CHIRON	618	610
HIP 52736	6748.52	CHIRON	530	540
HIP 52736	6713.70	CHIRON	263	490
HIP 52911	6670.86	TS23	758	1950
HR 4259	6335.70	CHIRON	304	330
HIP 54849	6670.94	TS23	797	2080
HIP 55434	6332.77	CHIRON	199	410
HIP 56034	6676.91	TS23	502	1460
HIP 56633	6669.91	TS23	447	1990
HIP 56633	6335.75	CHIRON	358	470
HIP 57328	6338.68	CHIRON	419	490
HIP 57328	6370.62	CHIRON	419	450
HIP 59819	6669.96	TS23	465	1940
HIP 60009	6370.66	CHIRON	200	520
HIP 60009	7009.78	CHIRON	206	510
HIP 60030	7084.81	IGRINS	2400	80
HIP 60595	6676.94	TS23	746	1540
HIP 60710	7062.77	CHIRON	1515	470
HIP 60957	6678.92	TS23	904	1500
HIP 61558	7139.67	IGRINS	1440	180
HIP 61558	7084.84	IGRINS	1200	70
HIP 61622	6378.69	CHIRON	167	620
HIP 62541	7124.80	IGRINS	480	120
HIP 62541	7084.86	IGRINS	1500	80
HIP 62576	7122.83	IGRINS	546	130
HIP 63724	6338.76	CHIRON	412	560
HIP 63724	6371.72	CHIRON	412	630
HIP 63945	6371.68	CHIRON	362	560
HIP 65198	7044.85	CHIRON	3352	430
HIP 65477	6670.01	TS23	207	2520
HIP 65728	6677.98	TS23	1200	1710
HIP 66249	6378.71	CHIRON	110	520
HIP 66798	6377.82	HRS	362	610
HIP 66821	6718.75	CHIRON	610	540
HIP 67143	7139.77	IGRINS	480	120
HIP 67194	6389.70	HRS	368	740
HIP 67782	6394.92	HRS	359	680
HIP 68092	7139.80	IGRINS	840	200
HIP 68520	6403.59	CHIRON	239	470
HIP 70327	7123.90	IGRINS	420	90
HIP 70327	6681.98	TS23	1152	230
HIP 70327	6719.80	CHIRON	368	460
HIP 70384	6403.73	HRS	420	560
HIP 70400	6669.00	TS23	602	2000
HIP 70915	7136.63	CHIRON	3281	480
HIP 70915	7090.71	CHIRON	2985	460
HIP 71865	6383.71	CHIRON	190	460
HIP 71865	7060.80	CHIRON	1205	500
HIP 71974	7078.80	CHIRON	3786	470
HIP 72104	6720.86	CHIRON	492	490
HIP 72154	6403.75	HRS	300	470
HIP 72250	7070.72	CHIRON	4025	490
HIP 72378	7139.82	IGRINS	720	140
HIP 72552	7124.81	IGRINS	600	110
HIP 73049	6715.73	CHIRON	749	530
HR 5605	6383.74	CHIRON	330	530
HIP 74117	6383.77	CHIRON	204	370
HIP 74689	6872.52	CHIRON	693	550

TABLE 2 — *Continued*

star	MJD (JD-2450000)	instrument	exptime (sec)	snr
HIP 75178	6678.99	TS23	815	1620
HIP 75304	6427.78	CHIRON	309	340
HIP 76267	6380.88	CHIRON	36	290
HIP 76600	6380.91	CHIRON	137	500
HIP 76852	6426.65	CHIRON	306	370
HIP 77233	6426.69	CHIRON	140	320
HIP 77336	6396.79	HRS	264	610
HIP 77336	7122.91	IGRINS	480	120
HIP 77516	6380.89	CHIRON	126	450
HIP 77635	6725.72	CHIRON	288	420
HIP 77858	6733.75	CHIRON	628	490
HIP 78105	6870.54	CHIRON	655	590
HIP 78106	6736.70	CHIRON	584	500
HIP 78265	6766.77	CHIRON	22	250
HIP 78554	6427.74	CHIRON	408	270
HIP 78820	6380.93	CHIRON	53	490
HIP 78820	7139.83	IGRINS	120	190
HIP 78820	7060.85	CHIRON	263	360
HIP 78820	7156.63	CHIRON	164	390
HR 6025	6847.83	IGRINS	600	100
HIP 78918	6718.86	CHIRON	300	610
HIP 78933	6737.76	CHIRON	77	250
HIP 79005	7090.77	CHIRON	4646	430
HIP 79007	6874.48	CHIRON	659	550
HIP 79199	6734.71	CHIRON	451	470
HIP 79387	6746.75	CHIRON	573	500
HIP 79404	6415.77	CHIRON	324	470
HIP 79404	7076.81	CHIRON	1307	430
HIP 79404	7090.88	CHIRON	1135	450
HIP 79653	6740.79	CHIRON	469	490
HIP 80460	7122.93	IGRINS	720	110
HIP 80815	6378.86	CHIRON	393	530
HIP 80883	6378.84	CHIRON	174	550
HIP 80991	6389.86	HRS	404	720
HIP 81126	7122.95	IGRINS	720	150
HIP 81641	6404.83	HRS	320	540
HIP 82350	6391.84	HRS	404	660
HIP 82514	6726.81	CHIRON	34	250
HIP 82673	6871.58	CHIRON	250	310
HIP 82673	6410.86	CHIRON	272	180
HIP 83635	6407.86	HRS	316	480
HIP 84606	6945.54	IGRINS	224	150
HIP 85290	6946.56	IGRINS	224	120
HIP 85379	6398.85	HRS	330	740
HIP 85385	6848.83	IGRINS	480	80
HIP 85537	7096.88	CHIRON	4227	570
HIP 85537	6792.73	CHIRON	900	600
HIP 85537	6848.73	IGRINS	240	60
HIP 85727	6771.85	CHIRON	175	570
HIP 85922	6847.82	IGRINS	480	120
HIP 85922	7139.95	IGRINS	240	170
HIP 85922	6886.56	CHIRON	791	590
HIP 85922	7103.85	CHIRON	2543	370
HIP 85922	7104.82	CHIRON	7386	360
HIP 86019	6747.85	CHIRON	228	510
HIP 86782	6404.85	HRS	310	500
HIP 87108	6847.87	IGRINS	120	120
HIP 87108	6445.79	CHIRON	152	300
HIP 88116	6848.71	CHIRON	373	590
HIP 88116	6876.54	CHIRON	320	380
HIP 88290	6873.59	CHIRON	365	540
HIP 88818	7122.98	IGRINS	960	90
HIP 88818	7230.66	IGRINS	600	110
HIP 88818	6397.85	HRS	355	510
HIP 88817	7123.00	IGRINS	960	100
HIP 88817	6405.84	HRS	400	720
HIP 89156	6405.82	HRS	470	610
HIP 89935	6848.85	IGRINS	240	100
HIP 89935	6945.56	IGRINS	224	250
HIP 90052	6405.88	HRS	500	760
HIP 90762	6848.85	IGRINS	480	80
HIP 90762	6945.57	IGRINS	480	200
HIP 90887	6748.80	CHIRON	710	560
HIP 91118	6945.58	IGRINS	360	190
HIP 91875	6745.81	CHIRON	680	580
HIP 92027	6405.91	HRS	360	570

TABLE 2 — *Continued*

star	MJD (JD-2450000)	instrument	exptime (sec)	snr
HIP 92312	6408.88	HRS	390	650
HIP 92728	6405.86	HRS	280	560
HIP 92855	6880.57	CHIRON	30	550
HIP 92855	6415.80	CHIRON	32	400
HIP 92946	6475.79	CHIRON	339	500
HIP 93225	6946.54	IGRINS	224	80
HIP 93225	6516.69	CHIRON	1200	540
HIP 93225	6962.56	TS23	562	1430
HIP 93393	6404.88	HRS	320	540
HIP 93580	7116.84	CHIRON	5594	520
HIP 93580	6848.84	IGRINS	480	100
HIP 93713	6848.87	IGRINS	600	90
HIP 93747	6587.54	TS23	85	1880
HIP 93805	6852.82	IGRINS	2640	60
HIP 93805	7139.96	IGRINS	120	210
HIP 93805	6775.78	CHIRON	150	520
HIP 94620	6848.88	IGRINS	480	100
HIP 94720	6517.78	HRS	400	880
HIP 95241	6869.63	CHIRON	325	120
HIP 95241	6508.80	CHIRON	294	600
HIP 95241	6459.89	CHIRON	183	360
HIP 95560	6848.89	IGRINS	480	110
HIP 95619	7139.97	IGRINS	480	120
HIP 95619	7118.79	CHIRON	3451	320
HIP 95619	6523.61	CHIRON	768	670
HIP 95853	6585.54	TS23	129	2010
HIP 96288	6585.56	TS23	489	1860
HIP 96840	6408.92	HRS	552	940
HIP 97376	6848.90	IGRINS	1680	70
HIP 97496	6584.54	TS23	342	1820
HIP 97870	6517.81	HRS	185	830
HIP 97966	6925.51	CHIRON	655	380
HIP 97966	6881.70	CHIRON	1158	660
HIP 98055	6586.54	TS23	320	1820
HIP 98325	6587.56	TS23	543	1750
HIP 99080	6583.63	TS23	358	1740
HIP 99742	6945.59	IGRINS	224	210
HIP 100069	6409.91	HRS	451	560
HIP 100221	7230.72	IGRINS	1100	80
HIP 100221	6523.79	HRS	874	830
HIP 100907	6946.57	IGRINS	224	120
HIP 100907	7230.67	IGRINS	600	120
HIP 101123	6945.70	IGRINS	224	160
HIP 101589	6448.83	CHIRON	352	420
HIP 101716	6582.60	TS23	549	1260
HIP 101909	6945.60	IGRINS	360	140
HIP 101909	7230.69	IGRINS	720	90
HIP 102487	6847.80	IGRINS	480	80
HIP 103298	6946.58	IGRINS	224	100
HIP 103298	7230.70	IGRINS	600	80
HIP 103298	7155.93	CHIRON	1141	290
HIP 104105	6945.69	IGRINS	280	140
HIP 104139	6448.90	CHIRON	204	490
HIP 104365	6847.81	IGRINS	480	100
HIP 104365	7237.82	IGRINS	720	50
HIP 105140	6485.90	CHIRON	372	420
HIP 105282	6522.65	HRS	1006	850
HIP 105891	6946.59	IGRINS	224	90
HIP 105942	6523.87	HRS	480	760
HIP 105966	6585.64	TS23	530	1800
HIP 105972	6507.82	HRS	267	690
HIP 106711	6584.60	TS23	689	700
HIP 106711	6618.53	TS23	557	2010
HIP 106786	6945.64	IGRINS	224	230
HIP 106786	6962.59	TS23	284	1620
HIP 106786	6794.81	CHIRON	232	470
HIP 107517	6873.74	CHIRON	1025	490
HIP 107608	6788.84	CHIRON	620	470
HIP 108294	6790.81	CHIRON	470	510
HIP 108339	6945.65	IGRINS	224	160
HIP 109056	6945.66	IGRINS	240	150
HIP 109056	6948.56	IGRINS	1156	160
HIP 109056	6946.65	IGRINS	784	230
HIP 109056	6947.57	IGRINS	1746	170
HIP 109139	6524.67	CHIRON	207	590
HIP 109139	6447.91	CHIRON	248	470

TABLE 2 — *Continued*

star	MJD (JD-2450000)	instrument	exptime (sec)	snr
HIP 109521	6586.58	TS23	511	1860
HIP 109521	6962.60	TS23	587	1500
HIP 109521	6945.68	IGRINS	224	200
HIP 109831	6945.67	IGRINS	224	160
HIP 109831	7237.77	IGRINS	1440	100
HIP 109831	7288.73	IGRINS	900	30
HIP 110838	6543.82	CHIRON	506	550
HIP 110838	6880.76	CHIRON	354	780
HIP 110935	6896.67	CHIRON	696	630
HIP 111056	7288.80	IGRINS	180	30
HIP 111056	6945.76	IGRINS	224	120
HIP 111068	6512.74	HRS	362	500
HIP 111169	6585.62	TS23	121	1900
HIP 112029	6487.85	CHIRON	109	460
HIP 112029	6892.74	CHIRON	95	250
HIP 113788	6586.63	TS23	367	1830
HIP 114520	6587.64	TS23	541	1880
HIP 114822	6886.68	CHIRON	715	550
HIP 114822	6884.68	CHIRON	530	530
HIP 115115	7163.90	CHIRON	600	190
HIP 115115	7230.95	IGRINS	500	40
HIP 115115	6797.87	CHIRON	610	330
HIP 116247	6463.89	CHIRON	368	560
HIP 116247	7237.94	IGRINS	240	100
HIP 116582	6510.77	HRS	534	670
HIP 116611	6946.61	IGRINS	224	140
HIP 116631	6962.63	TS23	249	1980
HIP 116631	6946.78	IGRINS	224	160
HIP 116631	6583.71	TS23	162	1740
HIP 116631	7288.80	IGRINS	180	30
HIP 116805	6528.84	TS23	158	1680
HIP 116971	6527.85	TS23	407	1650
HIP 116971	6487.88	CHIRON	298	540
HIP 116971	6555.56	CHIRON	497	430
HIP 116971	6869.76	CHIRON	380	110
HIP 116971	6936.73	CHIRON	344	600
HIP 117089	7288.81	IGRINS	180	20
HIP 117089	7237.95	IGRINS	720	60
HIP 117089	6513.86	CHIRON	853	600
HIP 117371	6586.67	TS23	349	1760
HIP 117452	6469.90	CHIRON	327	540
HIP 118121	6795.86	CHIRON	233	500
HIP 118243	6945.73	IGRINS	224	170
HIP 118243	6583.74	TS23	351	1760

NOTE. — See Section 2.1 for details of the signal-to-noise ratio calculation (the snr column)

TABLE 3
 NIRI OBSERVATION LOG

star	K	date	Exposure	ρ	θ	ΔK_c	$M_2(M_\odot)$	a (AU)
HIP 22833	4.83	2015-03-29	50x0.3	0.352 + / - 0.003	14.1 ± 0.7	3.04 ± 0.06	0.9 ^{+0.16} _{-0.17}	25.1 ± 0.24
HIP 22958	5.79	2015-10-19	52x0.4	0.445 + / - 0.003	65.0 ± 0.3	2.57 ± 0.05	1.5 ^{+0.35} _{-0.28}	124.1 ± 0.81
HIP 26093	5.96	2015-03-23	33x0.6
HIP 26126	5.07	2015-03-29	40x0.4
HIP 29735	5.10	2015-03-22	83x0.2
HIP 31278	5.46	2015-03-28	29x0.6
HIP 38538	4.66	2015-10-19	75x0.2
HIP 39847	4.66	2015-03-27	50x0.3
HIP 75178	5.49	2015-03-24	29x0.6
HIP 88116	4.47	2015-03-22	50x0.3	3.671 + / - 0.001	242.99 ± 0.02	3.9 ± 0.4	1.2 ^{+0.28} _{-0.24}	467.7 ± 0.18
HIP 91118	5.67	2015-10-16	43x0.4	0.1667 + / - 0.0007	41.7 ± 0.2	1.77 ± 0.01	1.5 ^{+0.39} _{-0.25}	36.4 ± 0.16
HIP 100221	5.70	2015-10-18	26x0.7	0.250 + / - 0.002	346.8 ± 0.92	2.28 ± 0.04	0.9 ^{+0.2} _{-0.23}	28.5 ± 0.24
HIP 100907	5.41	2015-10-16	43x0.4	0.463 + / - 0.002	335.4 ± 0.30	2.91 ± 0.04	0.7 ^{+0.14} _{-0.10}	37.7 ± 0.16
HIP 101909	6.47 [†]	2015-10-16	39x0.5
HIP 109139	4.40	2015-04-26	50x0.3
HIP 109521	4.96	2015-04-25	40x0.4
HIP 115115	4.96	2015-10-18	40x0.4	1.497 + / - 0.002	313.14 ± 0.08	2.54 ± 0.04	1.3 ^{+0.28} _{-0.19}	120.0 ± 0.17

NOTE. — [†]: There is no K-magnitude tabulated in the Simbad Database. The value quoted here is estimated from the spectral type of the star and its V-band magnitude.

TABLE 4
 COMPANION DETECTIONS

star	component	N_{obs}	Used in Analysis	T_{eff} (K)	$v \sin i$ (km s $^{-1}$)	[Fe/H] (dex)	Mass (M_{\odot}) Isochrone	Spectral Type
HIP 2548	Aa,Ab	2	yes	5732 ± 112	30	-0.5	$1.0^{+0.06}_{-0.04}$	$1.0^{+0.04}_{-0.03}$
HIP 5348	AB	1	no	12000 ± 1000	75	0.0	$2.9^{+0.40}_{-0.36}$	$3.3^{+0.23}_{-0.29}$
HR 545	Aa,Ab †	3	yes	4312 ± 87	5	-0.5	$0.8^{+0.11}_{-0.10}$	$0.7^{+0.01}_{-0.02}$
HR 604	AB	1	no	4736 ± 150	5	0.5	$0.9^{+0.17}_{-0.12}$	$0.8^{+0.02}_{-0.02}$
HIP 10732	AB †	2	yes	5578 ± 109	5	0.0	$1.0^{+0.04}_{-0.03}$	$1.0^{+0.04}_{-0.04}$
HIP 12332	AB †	2	yes	5551 ± 107	10	0.0	$1.0^{+0.03}_{-0.03}$	$1.0^{+0.04}_{-0.04}$
HIP 12706	AB	2	yes	6051 ± 107	10	0.0	$1.1^{+0.31}_{-0.03}$	$1.1^{+0.04}_{-0.05}$
HIP 13165	Aa,Ab	1	no	5773 ± 163	5	-0.5	$1.1^{+0.31}_{-0.08}$	$1.0^{+0.10}_{-0.03}$
HIP 13327	AB †	1	yes	5524 ± 150	5	-0.5	$1.2^{+0.20}_{-0.21}$	$1.0^{+0.03}_{-0.04}$
HIP 14043	Aa,Ab †	1	yes	11500 ± 500	20	0.5	$2.6^{+0.36}_{-0.29}$	$3.3^{+0.15}_{-0.67}$
HIP 14764	AB †	2	yes	5623 ± 150	5	-0.5	$1.0^{+0.32}_{-0.07}$	$1.0^{+0.03}_{-0.04}$
HIP 16147	AB	1	yes	13000 ± 1000	1	0.0	$3.1^{+0.38}_{-0.36}$	$3.6^{+0.34}_{-0.23}$
HIP 16244	AB	2	yes	5592 ± 107	5	-0.5	$1.2^{+0.20}_{-0.22}$	$1.0^{+0.03}_{-0.03}$
HIP 16340	AB †	1	yes	6214 ± 150	5	-0.5	$1.2^{+0.29}_{-0.07}$	$1.2^{+0.06}_{-0.05}$
HIP 16611	AB	1	yes	11500 ± 1000	75	0.0	$2.7^{+0.47}_{-0.37}$	$3.3^{+0.15}_{-0.66}$
HIP 19949	AB †	1	yes	6492 ± 155	20	-0.5	$1.3^{+0.06}_{-0.05}$	$1.3^{+0.06}_{-0.06}$
HIP 20380	AB †	2	yes	6492 ± 109	20	-0.5	$1.3^{+0.04}_{-0.04}$	$1.3^{+0.03}_{-0.05}$
HIP 21589	Aa,Ab	1	yes	4562 ± 154	5	0.0	$0.7^{+0.04}_{-0.03}$	$0.8^{+0.02}_{-0.03}$
HIP 22833	AB	2	yes	4745 ± 107	10	0.0	$0.8^{+0.02}_{-0.02}$	$0.8^{+0.02}_{-0.01}$
HIP 22958	Aa,Ab	2	yes	5762 ± 158	30	-0.5	$1.3^{+0.19}_{-0.23}$	$1.0^{+0.09}_{-0.03}$
HIP 23362	AB †	1	yes	6283 ± 158	5	-0.5	$1.2^{+0.06}_{-0.05}$	$1.2^{+0.07}_{-0.05}$
HIP 24902	AB	1	yes	5679 ± 154	30	0.0	$1.0^{+0.05}_{-0.04}$	$1.0^{+0.04}_{-0.03}$
HIP 26126	AB?	3	yes	5841 ± 91	5	-0.5	$1.0^{+0.03}_{-0.03}$	$1.0^{+0.05}_{-0.04}$
HIP 28691	AB	1	no	15000 ± 1000	1	0.5	$4.0^{+0.45}_{-0.43}$	$4.2^{+0.43}_{-0.34}$
HIP 28691	AC	1	no	12000 ± 1000	1	0.5	$2.8^{+0.40}_{-0.34}$	$3.3^{+0.23}_{-0.39}$
HIP 32607	AB †	3	yes	5068 ± 91	5	-0.5	$0.8^{+0.02}_{-0.02}$	$0.9^{+0.01}_{-0.01}$
HIP 37322	AB	1	yes	8157 ± 147	30	-0.5	$1.8^{+0.30}_{-0.07}$	$1.9^{+0.01}_{-0.07}$
HIP 37450	AB †	1	yes	16000 ± 1000	30	0.0	$4.3^{+0.36}_{-0.43}$	$4.7^{+0.71}_{-0.39}$
HIP 38538	AB	1	no	6576 ± 150	75	0.0	$1.3^{+0.05}_{-0.05}$	$1.3^{+0.09}_{-0.05}$
HIP 38593	AB †	2	yes	5398 ± 112	5	-0.5	$1.3^{+0.08}_{-0.13}$	$0.9^{+0.03}_{-0.03}$
HIP 38846	AB †	1	yes	6595 ± 158	10	0.0	$1.7^{+0.12}_{-0.21}$	$1.3^{+0.09}_{-0.05}$
HIP 39847	Aa,Ab †	2	no	5750 ± 107	10	-0.5	$1.0^{+0.04}_{-0.03}$	$1.0^{+0.05}_{-0.03}$
HIP 40881	AB †	1	yes	4562 ± 154	10	-0.5	$0.8^{+0.18}_{-0.05}$	$0.8^{+0.02}_{-0.03}$
HIP 42129	AB	1	yes	5241 ± 158	10	-0.5	$1.2^{+0.12}_{-0.18}$	$0.9^{+0.04}_{-0.02}$
HIP 46283	AB?	3	yes	9268 ± 85	10	0.5	$2.0^{+0.04}_{-0.02}$	$2.2^{+0.02}_{-0.02}$
HIP 52678	AB †	2	yes	5033 ± 112	10	-0.5	$1.0^{+0.15}_{-0.19}$	$0.8^{+0.01}_{-0.02}$
HIP 63945	AC	1	no	7038 ± 162	10	-0.5	$1.6^{+0.26}_{-0.16}$	$1.5^{+0.08}_{-0.06}$
HIP 72154	AB †	1	yes	4918 ± 162	30	-0.5	$0.9^{+0.22}_{-0.09}$	$0.8^{+0.03}_{-0.03}$
HR 5605	AB	1	no	16000 ± 1000	10	0.0	$4.3^{+0.37}_{-0.42}$	$4.7^{+0.76}_{-0.40}$
HR 5605	AC	1	no	14000 ± 1000	10	0.0	$3.5^{+0.42}_{-0.38}$	$3.9^{+0.35}_{-0.34}$
HIP 74117	AB	1	no	14000 ± 1000	10	0.0	$3.5^{+0.42}_{-0.38}$	$3.9^{+0.34}_{-0.34}$
HIP 76267	AB	1	yes	5449 ± 158	5	-0.5	$0.9^{+0.04}_{-0.04}$	$0.9^{+0.04}_{-0.03}$
HIP 77336	AB †	2	yes	6407 ± 112	20	0.0	$1.2^{+0.04}_{-0.04}$	$1.3^{+0.04}_{-0.05}$
HIP 77516	AB	1	yes	6825 ± 141	5	0.5	$1.4^{+0.21}_{-0.06}$	$1.4^{+0.03}_{-0.04}$
HIP 78820	AB	1	no	5658 ± 158	5	0	$1.3^{+0.11}_{-0.13}$	$1.0^{+0.04}_{-0.04}$
HIP 78918	AB	1	yes	9000 ± 500	120	-0.5	$2.0^{+0.22}_{-0.17}$	$2.1^{+0.13}_{-0.17}$
HIP 79199	AB	1	no	4616 ± 158	5	-0.5	$0.9^{+0.14}_{-0.14}$	$0.8^{+0.02}_{-0.03}$
HIP 79404	AB †	2	yes	4773 ± 112	10	-0.5	$1.1^{+0.07}_{-0.08}$	$0.8^{+0.02}_{-0.01}$
HIP 80460	AB	1	yes	6391 ± 155	10	0.0	$1.2^{+0.06}_{-0.05}$	$1.3^{+0.06}_{-0.06}$
HIP 82673	AB †	2	yes	4668 ± 112	5	0.5	$0.8^{+0.03}_{-0.03}$	$0.8^{+0.01}_{-0.02}$
HIP 84606	AB	1	yes	5476 ± 154	10	-0.5	$0.9^{+0.05}_{-0.04}$	$0.9^{+0.04}_{-0.03}$
HIP 88116	AB †	2	yes	5293 ± 112	5	0.0	$0.9^{+0.03}_{-0.03}$	$0.9^{+0.02}_{-0.03}$
HIP 88817	Ba,Bb †	1	yes	3647 ± 154	20	0.0	$0.5^{+0.07}_{-0.10}$	$0.5^{+0.03}_{-0.05}$
HIP 88818	Aa,Ab	3	yes	5296 ± 91	20	-0.5	$0.9^{+0.02}_{-0.02}$	$0.9^{+0.02}_{-0.03}$
HIP 91118	AB	1	yes	6492 ± 155	10	-0.5	$1.3^{+0.26}_{-0.07}$	$1.3^{+0.06}_{-0.06}$
HIP 93225	AB	2	yes	14000 ± 700	10	0.5	$3.6^{+0.34}_{-0.30}$	$3.9^{+0.18}_{-0.23}$
HIP 93805	Aa,Ab †	2	yes	4054 ± 109	5	-0.5	$0.6^{+0.03}_{-0.03}$	$0.6^{+0.04}_{-0.02}$

TABLE 4 — *Continued*

star	component	N_{obs}	Used in Analysis	T_{eff} (K)	$v \sin i$ (km s $^{-1}$)	[Fe/H] (dex)	Isochrone	Mass (M_{\odot})	Spectral Type
HIP 96840	AB	1	yes	9942 ± 152	10	0.0	$2.2^{+0.06}_{-0.05}$	$2.3^{+0.03}_{-0.01}$	
HIP 100221	AB	1	yes	5273 ± 154	20	-0.5	$0.9^{+0.29}_{-0.07}$	$0.9^{+0.04}_{-0.03}$	
HIP 100907	AB †	2	yes	5222 ± 109	10	0.0	$0.9^{+0.03}_{-0.03}$	$0.9^{+0.04}_{-0.02}$	
HIP 103298	Aa,Ab	3	yes	4615 ± 90	5	-0.5	$0.7^{+0.02}_{-0.02}$	$0.8^{+0.01}_{-0.02}$	
HIP 109139	AB	2	yes	5710 ± 112	20	-0.5	$1.0^{+0.04}_{-0.03}$	$1.0^{+0.03}_{-0.03}$	
HIP 109521	Aa,Ab †	3	yes	4412 ± 87	10	0.0	$0.7^{+0.02}_{-0.02}$	$0.7^{+0.01}_{-0.01}$	
HIP 115115	AB	3	yes	4943 ± 91	5	-0.5	$0.8^{+0.02}_{-0.02}$	$0.8^{+0.02}_{-0.02}$	

NOTE. — \dagger : Newly discovered companions.

TABLE 5
MASS-RATIO DISTRIBUTION PARAMETERS.

Model	Parameter	Median Value	1 σ credible interval	
			Lower	Upper
Histogram	θ_1	0.50	0.18	1.00
	θ_2	1.53	1.14	1.89
	θ_3	2.17	1.80	2.65
	θ_4	1.42	0.98	1.81
	θ_5	0.74	0.40	1.12
	θ_6	0.29	0.10	0.55
	θ_7	0.16	0.06	0.33
Lognormal	μ	-0.99	-1.06	-0.92
	σ	0.46	0.40	0.54
	maximum [†]	0.30	0.27	0.33
Power Law	γ	0.29	0.15	0.42

NOTE. — [†]: This parameter is derived from the mean and standard deviation, not fit.

REFERENCES

- Anderson, T. W., & Darling, D. A. 1954, Journal of the American Statistical Association, 49, 765
- Andrews, S. M., Rosenfeld, K. A., Kraus, A. L., & Wilner, D. J. 2013, ApJ, 771, 129
- Aydi, E., Gebran, M., Monier, R., et al. 2014, in SF2A-2014: Proceedings of the Annual meeting of the French Society of Astronomy and Astrophysics, ed. J. Ballet, F. Martins, F. Bournaud, R. Monier, & C. Reylé, 451–455
- Barnes, S. A. 2010, ApJ, 722, 222
- Barnes, S. A., & Kim, Y.-C. 2010, ApJ, 721, 675
- Bate, M. R. 2012, MNRAS, 419, 3115
- Bate, M. R., & Bonnell, I. A. 1997, MNRAS, 285, 33
- Bate, M. R., Bonnell, I. A., & Bromm, V. 2002, MNRAS, 336, 705
- Bate, M. R., Bonnell, I. A., & Price, N. M. 1995, MNRAS, 277, 362
- Binney, J., & Merrifield, M. 1998, Galactic Astronomy
- Boss, A. P. 1986, ApJS, 62, 519
- Boss, A. P., & Bodenheimer, P. 1979, ApJ, 234, 289
- Bouvier, J., Matt, S. P., Mohanty, S., et al. 2014, Protostars and Planets VI, 433
- Bressan, A., Marigo, P., Girardi, L., et al. 2012, MNRAS, 427, 127
- Castelli, F., & Kurucz, R. L. 2003, in IAU Symposium, Vol. 210, Modelling of Stellar Atmospheres, ed. N. Piskunov, W. W. Weiss, & D. F. Gray, 20P
- David, T. J., & Hillenbrand, L. A. 2015, ArXiv e-prints, arXiv:1501.03154
- De Rosa, R. J., Patience, J., Wilson, P. A., et al. 2014, MNRAS, 437, 1216
- Delfosse, X., Beuzit, J.-L., Marchal, L., et al. 2004, in Astronomical Society of the Pacific Conference Series, Vol. 318, Spectroscopically and Spatially Resolving the Components of the Close Binary Stars, ed. R. W. Hilditch, H. Hensberge, & K. Pavlovski, 166–174
- Dotter, A., Chaboyer, B., Jevremović, D., et al. 2008, ApJS, 178, 89
- Duchêne, G., & Kraus, A. 2013, ARA&A, 51, 269
- Duquennoy, A., & Mayor, M. 1991, A&A, 248, 485
- Feroz, F., Hobson, M. P., Cameron, E., & Pettitt, A. N. 2013, ArXiv e-prints, arXiv:1306.2144
- Fischer, D. A., & Marcy, G. W. 1992, ApJ, 396, 178
- Foreman-Mackey, D., Hogg, D. W., & Morton, T. D. 2014, ApJ, 795, 64
- Gullikson, K., Dodson-Robinson, S., & Kraus, A. 2014, AJ, 148, 53
- Gullikson, K., Kraus, A., Dodson-Robinson, S., et al. 2016, AJ, 151, 3
- Horne, K. 1986, PASP, 98, 609
- Husser, T.-O., Wende-von Berg, S., Dreizler, S., et al. 2013, A&A, 553, A6
- Kouwenhoven, M. B. N., Brown, A. G. A., Portegies Zwart, S. F., & Kaper, L. 2007, A&A, 474, 77
- Kratter, K. M., & Matzner, C. D. 2006, MNRAS, 373, 1563
- Kratter, K. M., Matzner, C. D., Krumholz, M. R., & Klein, R. I. 2010, ApJ, 708, 1585
- Kroupa, P. 2002, Science, 295, 82
- Krumholz, M. R., Klein, R. I., & McKee, C. F. 2012, ApJ, 754, 71
- Lee, J.-J. 2015, plp: Version 2.0, doi:10.5281/zenodo.18579
- Mason, B. D., Wycoff, G. L., Hartkopf, W. I., Douglass, G. G., & Worley, C. E. 2014, VizieR Online Data Catalog, 1, 2026
- Moffat, A. F. J. 1969, A&A, 3, 455
- Morton, T. D. 2015, isochrones: Stellar model grid package, Astrophysics Source Code Library, ascl:1503.010
- Park, C., Jaffe, D. T., Yuk, I.-S., et al. 2014, in Society of Photo-Optical Instrumentation Engineers (SPIE) Conference Series, Vol. 9147, Society of Photo-Optical Instrumentation Engineers (SPIE) Conference Series, 1
- Parker, R. J., & Reggiani, M. M. 2013, MNRAS, 432, 2378
- Pecaut, M. J., & Mamajek, E. E. 2013, ApJS, 208, 9
- Pinsonneault, M. H., DePoy, D. L., & Coffee, M. 2001, ApJ, 556, L59
- Pourbaix, D., Tokovinin, A. A., Batten, A. H., et al. 2009, VizieR Online Data Catalog, 1, 2020
- Raghavan, D., McAlister, H. A., Henry, T. J., et al. 2010, ApJS, 190, 1
- Reggiani, M., & Meyer, M. R. 2013, A&A, 553, A124
- Reggiani, M. M., & Meyer, M. R. 2011, ApJ, 738, 60
- Stamatellos, D., & Whitworth, A. 2011, Research, Science and Technology of Brown Dwarfs and Exoplanets: Proceedings of an International Conference held in Shanghai on Occasion of a Total Eclipse of the Sun, Shanghai, China, Edited by E.L. Martin; J. Ge; W. Lin; EPJ Web of Conferences, Volume 16, id.05001, 16, 5001
- Tokovinin, A., Fischer, D. A., Bonati, M., et al. 2013, PASP, 125, 1336
- Tull, R. G. 1998, in Society of Photo-Optical Instrumentation Engineers (SPIE) Conference Series, Vol. 3355, Optical Astronomical Instrumentation, ed. S. D'Odorico, 387–398
- Tull, R. G., MacQueen, P. J., Sneden, C., & Lambert, D. L. 1995, PASP, 107, 251
- van Leeuwen, F. 2007, A&A, 474, 653
- Vuissoz, C., & Debernardi, Y. 2004, in Astronomical Society of the Pacific Conference Series, Vol. 318, Spectroscopically and Spatially Resolving the Components of the Close Binary Stars, ed. R. W. Hilditch, H. Hensberge, & K. Pavlovski, 320–322
- Wenger, M., Ochsenbein, F., Egret, D., et al. 2000, A&AS, 143, 9
- Zhao, B., & Li, Z.-Y. 2013, ApJ, 763, 7
- Zinnecker, H., & Yorke, H. W. 2007, ARA&A, 45, 481
- Zorec, J., & Royer, F. 2012, A&A, 537, A120
- Zucker, S. 2003, MNRAS, 342, 1291